Distribution Categories:
Coal Conversion and Utilization--
Advanced Power (UC-90f)
Coal Conversion and Utilization--
Materials and Components (UC-90h)

ANL-85-61

ANL--85-61

DE86 002550

ARGONNE NATIONAL LABORATORY
9700 South Cass Avenue
Argonne, Illinois 60439

ON THE EXPERIMENTAL OPERATION OF A SODIUM HEAT PIPE

by

R. E. Holtz, G. A. McLennan, and E. R. Koehl

Components Technology Division

May 1985

Prepared for

U. S. Department of Energy
Morgantown Energy Technology Center

DISCLAIMER

TABLE OF CONTENTS

LIST OF FIGURES

LIST OF TABLES

ON THE EXPERIMENTAL OPERATION OF A SODIUM HEAT PIPE

by

R. E. Holtz, G. A. McLennan, and E. R. Koehl

ABSTRACT

This report documents the operation of a 28 inch long sodium heat pipe in the Heat Pipe Test Facility (HPTF) installed at Argonne National Laboratory. Experiment data were gathered to simulate conditions prototypic of both a fluidized bed coal combustor application and a space environment application. Both sets of experiment data show good agreement with the heat pipe analytical model. The heat transfer performance of the heat pipe proved reliable over a substantial period of operation and over much thermal cycling. Additional testing of longer heat pipes under controlled laboratory conditions will be necessary to determine performance limitations and to complete the design code validation.

1. INTRODUCTION

This report describes the testing and post-test examination of a high-temperature sodium heat pipe. The heat pipe was constructed from 2 in. nominal diameter pipe and was 28 in. long. Previous reports [1,2] contain information pertinent to heat pipe design considerations, heat pipe analyses and code development, conceptual design of coal-fired power systems, prototype liquid metal heat pipe development for fluidized-bed combustors (FBC), a description of the heat pipe test facility and early results of experiments.

The initial work [1] focused primarily on the use of heat pipes as a method of delivering heat from an FBC to a closed-cycle prime mover, such as a closed-cycle gas turbine or a Stirling cycle engine. The continuation of heat pipe testing was directed at the use of thermionics as the prime mover. Potential applications include the use of thermionics as a topping cycle in a coal plant or as a prime mover in a nuclear-reactor-driven space power system.

Substantial background information is contained in Refs. 1 and 2. Hence, this report addresses only the heat pipe test facility, the heat pipe, the experimental program, and post-test examination activities.

2. DESCRIPTION OF HEAT PIPE TEST FACILITY

2.1 DESIGN AND LAYOUT OF TEST APPARATUS

The Argonne National Laboratory (ANL) Heat Pipe Test Facility (HPTF) consists of a radio frequency (R-F) induction power supply, the heat pipe under test, a gas-coupled water calorimeter (GCWC), and temperature and coolant monitoring instrumentation. The HPTF is illustrated in Fig. 1.

2.1.1 R-F Heat Source

The power source is an R-F induction power supply capable of providing 25 kW of power at a nominal 450 kHz into an appropriate load, e.g., a heat pipe. The R-F source induces a current in the metal wall of the load from a water-cooled inductor (R-F induction coil) placed around the heat pipe. The heat pipe acts as a shorted turn in the secondary of a transformer in that the pipe wall provides a closed circuit that allows induced current circulation. The heat pipe appears as a predominately resistive load to the R-F generator, and the amount of induced power dissipated (I^2R heating) in the heat pipe (P_w),

$$P_w = I_w^2 R_w \quad \text{watts} , \tag{1}$$

is a function of the induction coil current, number of coil turns, heat pipe physical dimensions, and heat pipe electromagnetic properties. Since the heat pipe resistance R_w equals the resistance of the equivalent circumferential current path of cross section $\delta_w \ell_w$ and length πd_w (approximately), Eq. 1 can be written:

$$P_w = \frac{\pi d_w \rho_w}{\delta_w \ell_w} \cdot I_c^2 N_c^2 \quad \text{watts} , \tag{2}$$

where

I_c is the work coil current in amperes,

I_w is the heat pipe current in amperes,

R_w is the heat pipe resistance in ohms,

N_c is the number of work coil turns,

ρ_w is the heat pipe resistivity in μohm-cm,

d_w is the heat pipe outside diameter in cm,

δ_w is the equivalent heat pipe current depth in cm, and

ℓ_w is the length of heat pipe in cm.

The equivalent DC heat pipe current depth is defined as the depth at which the current density is equal to 36.7% of its surface value,

$$\delta_w = \left(\frac{\rho_w}{\pi \mu_w f} \right)^{1/2} \quad \text{cm} , \tag{3}$$

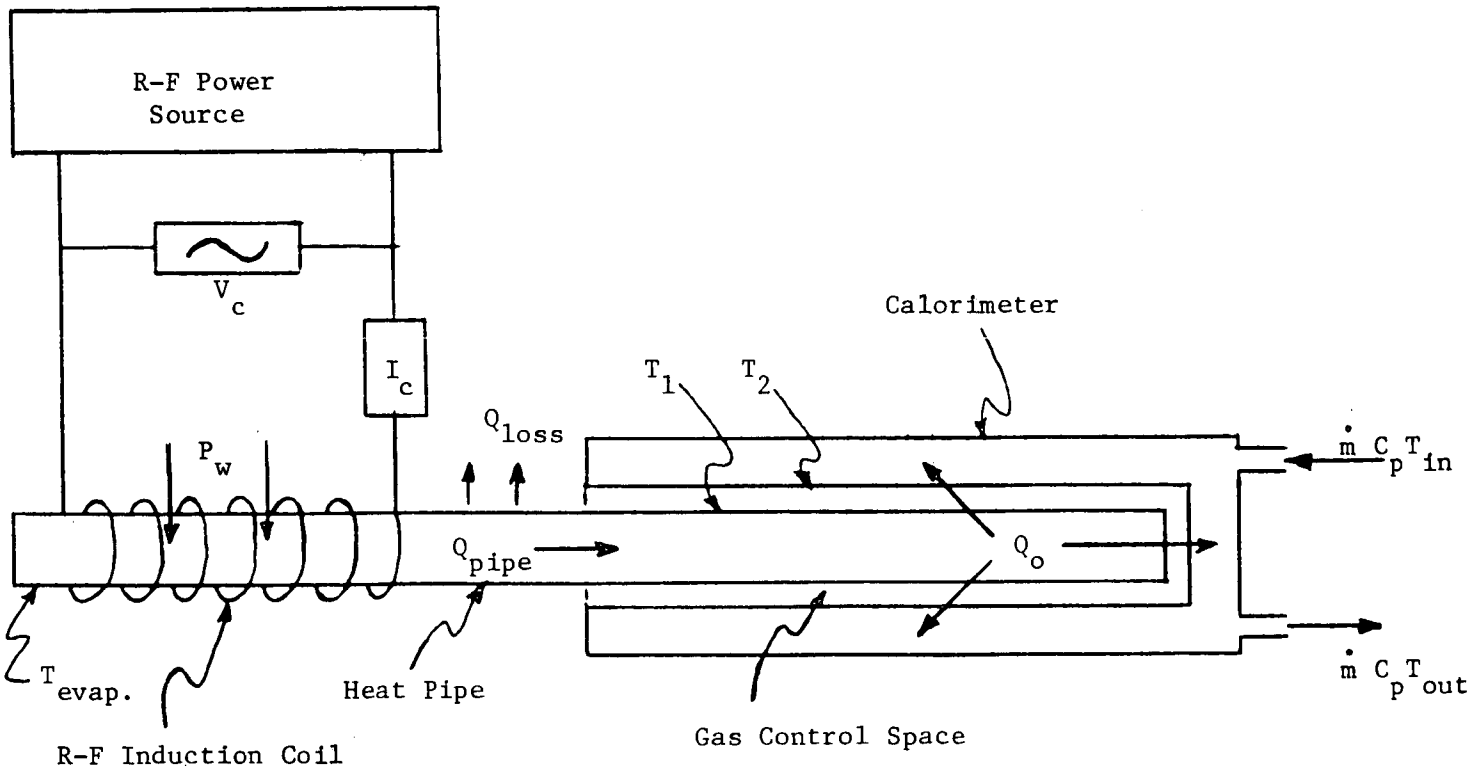

Fig. 1. Heat Pipe Test Facility

where ρ_w is the heat pipe resistivity in ohm-cm, μ_w is the permeability in henry/cm, and f is the operating frequency in Hz. For ANL's large Incoloy heat pipes and the 450 kHz R-F power source, δ_w = 0.084 cm, corresponding to ~30% of the pipe wall thickness.

The following are characteristics of induction heating:

- Surface or subsurface heating,
- Axial restriction of the R-F field to within the confines of the work coil,
- Extremely rapid heat transfer,
- Heat developed within the heat pipe itself,
- Mechanical and electrical isolation, and
- Extremely high heat pipe temperatures.

Additionally, induction heating eliminates concern over the outside evaporator surface heat transfer coefficient, thus allowing testing of the heat pipe at power levels that would otherwise be more difficult and/or more costly to achieve. Further, due to the rapid heating ability of induction heating, investigations of some of the more troublesome operating modes of the heat pipe are possible.

2.1.2 Gas-Water Calorimeter

The gas-coupled, water-cooled calorimeter is a non-contact method that enables the control of the heat transfer between two surfaces. It is especially effective for surfaces that have relatively low emissivities (e.g., polished metal surfaces). In the case of the HPTF experimental setup, heat is transferred from the heat pipe wall to the calorimeter by thermal radiation when the calorimeter enclosure is evacuated. If gas is added to the calorimeter the heat transfer is increased because of the effects of conduction and convection heat transfer being added to the thermal radiation heat transfer. A schematic of the calorimeter is shown in Fig. 2.

External connections to the calorimeter allow the evacuation of the space between the heat pipe and calorimeter surfaces, as well as the introduction of desired quantities and species of conducting gases into the space.

Minimum heat transfer in the calorimeter occurs when the space is evacuated and thermal radiation is the only mode of heat transfer that is occurring. In this case the heat transfer from the heat pipe to the calorimeter is

$$Q = \frac{\sigma A_1 \left(T_1^4 - T_2^4 \right)}{\frac{1}{\varepsilon_1} + \left[\frac{A_1}{A_2} \left(\frac{1}{\varepsilon_2} - 1 \right) \right]},$$

where

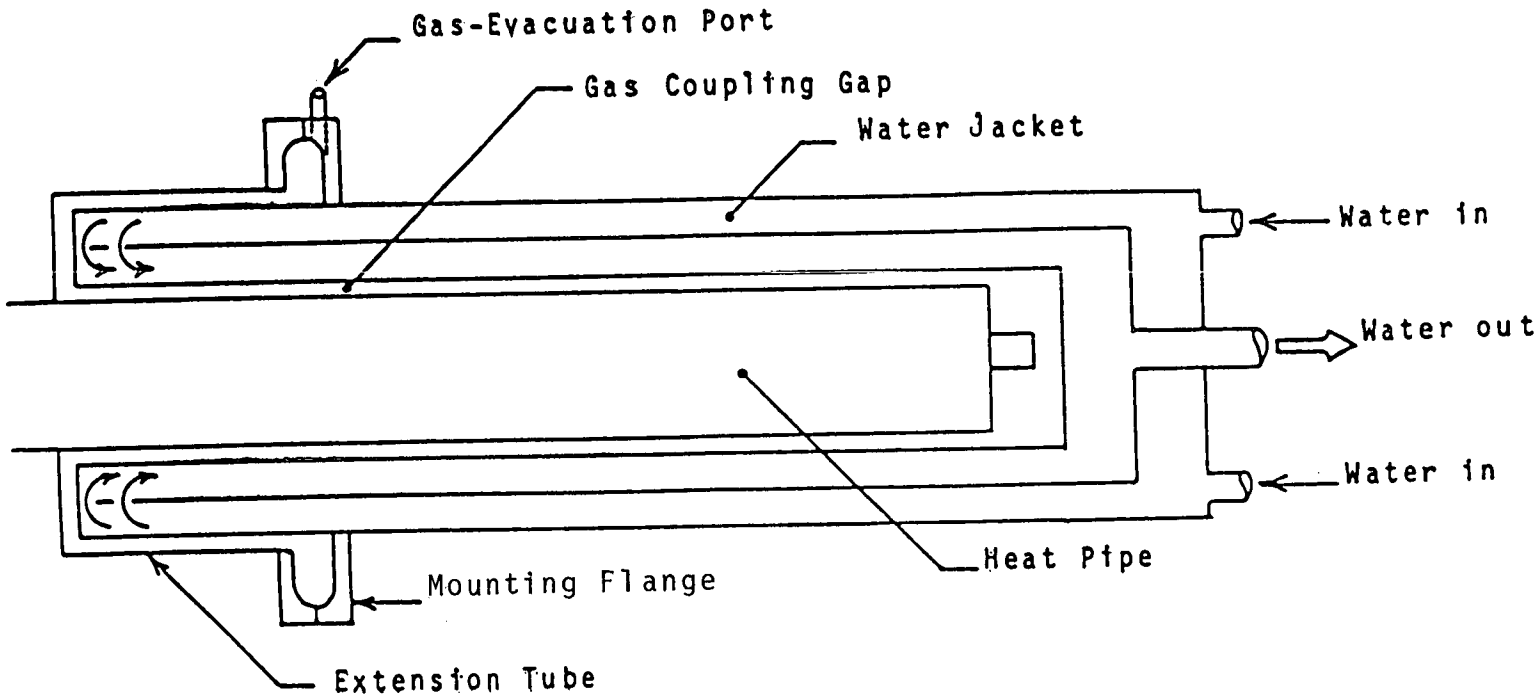

Fig. 2. Gas-Water Calorimeter

σ = Stefan Boltzman constant, 5.67×10^{-8} W/m^2·K^4,

A_1 = heat pipe condenser surface area, m^2,

A_2 = calorimeter surface area, m^2,

T_1 = heat pipe condenser surface temperature, K,

T_2 = calorimeter surface temperature, K,

ε_1 = heat pipe surface emissivity, and

ε_2 = calorimeter surface emissivity.

As gas is added to the space between the heat pipe and the calorimeter, the heat transfer between the heat pipe and calorimeter can be substantially increased. This coupling between the heat pipe and the calorimeter allows the simulation of various heat pipe operating environments such as:

- A fluidized bed combustor application, which will have combined thermal radiation, conduction, and convection, and
- An application in space, where thermal radiation is the only mode of heat transfer.

During operation of the HPTF, the energy transferred from the heat pipe to the calorimeter wall is conducted through the calorimeter wall (copper) and removed by a water stream. The heat removed by the water is:

$$Q_o = \dot{m}\ Cp\ \Delta T,$$

$\dot{m}$ = mass flowrate,

$\Delta T = T_{out} - T_{in}$ = water temperature, difference, and

Cp = water heat capacity.

The heat removed from the calorimeter, Q_o, is equal to the power input, P_w, at the evaporator less radiated losses in the adiabatic section and conduction losses at the heat pipe/calorimeter flange.

2.2 INSTRUMENTATION AND DATA ACQUISITION SYSTEM

Instrumentation for the HPTF consists of the following:

- Irtronics Model 3100BF non-contact infrared pyrometer with emissivity compensation--temperature range, 1200-1800°F, spectral range, 0.9-1.1 μ
- Acromag Model 319-BX-U differential, 3-wire RTD resistance bridge
- Omega Model PR-132, 100 ohm, 3-wire RTD temperature sensor
- Doric Model 410A digital temperature indicator--indicator range, 0.00-250.00°F ±0.02°F

- Type K thermocouple sensors, standard grade/accuracy
- Digital temperature indicator, range 0-1999°F
- Water flowmeter, range 0-10 gpm
- R-F voltage probe
- R-F current probe

This apparatus allows application of the previously stated power equations by measuring certain parameters of the heat pipe calorimeter system.

The pyrometer provides a baseline reference temperature for heat transfer calculations. The R-F probes are intended to provide input power information; the RTD bridge and water flow monitor provide output power information. Information on intermediate system losses is determined from the various thermocouples attached to the adiabatic section and the mounting flange.

The data acquisition system is a Hewlett Packard 21MX E Series 16-bit minicomputer-based system that operates a high-speed multichannel digital-to-analog converter for data acquisition. Data are stored on a 2.5 M byte removable disc cartridge and backup magnetic tape medium. The system executes Fortran code in real time, and can be used to provide startup and failsafe operation of the HPTF.

3. HEAT PIPE DESIGN AND FABRICATION

3.1 PROTOTYPE ELEMENT DESIGN

Two 70 cm (28 in.) long heat pipe units were fabricated. The selected heat pipe wall material was 2 in. IPS Schedule 10 Incoloy 800 pipe. The design temperature was 788°C (1450°F) at the exterior of the heat pipe evaporator. The average design power was 7800 W (27,000 Btuh). Thermacore computer program A37 was used to establish the wick structure, power handling capacity, and temperature difference of the heat pipe. The selected design for the first 70 cm heat pipe consisted of 2-1/2 wraps of 100 mesh screen lining the inside wall. Two longitudinal arteries of 3.18 mm (0.125 in.) ID were used to provide the necessary low-loss liquid return path. The 100 mesh wick served to distribute and collect the condensed sodium in the condenser and carry it circumferentially to the arteries. In the evaporator, the screen provided circumferential distribution of a thin film of sodium over the entire inside surface of the heat pipe. Specific dimensions, power limitations, and other details were calculated, using Thermacore's heat pipe design code. A design layout for both heat pipes is presented in Fig. 3. As discussed in Ref. 1, the heat pipe was protected from the corrosive and erosive effects of the FBC by coating it with a layer of FeCrAlY (Fecraly) and a layer of magnesium-zirconate. Accordingly, tests were conducted on samples of the selected Incoloy 800 pipe to validate the integrity of the bond between the coating and the underlying alloy.

Two Incoloy 800 samples 3 in. long x 2-3/8 in. OD were coated with Fecraly and magnesium-zirconate. One sample was heat-treated to 1652°F (850°C) by heating it very slowly in a vacuum. The second sample was heat-treated in air using the same heating schedule. The vacuum-treated sample was thermally cycled three times, using a slow heating and cooling cycle. Both samples were cycled eight times by putting the room temperature part in the furnace at 850°C, leaving them for one hour, and removing the hot samples directly into the air. Neither sample showed signs of any cracking or spalling of the coatings. Then both samples were heated to 850°C, removed, and plunged directly into cold water. Again, neither sample showed cracking or other signs of failure. The double-layered coatings showed no signs of failure on either sample, and bonding integrity was judged satisfactory.

3.2 FABRICATION

The first step in fabrication of the prototype heat pipe elements was to machine the parts from 2 in. IPS Schedule 10 (2-3/8 in. OD x 0.109 in. wall) Incoloy 800 (Type H) pipe. Following degreasing, the first wrap of 100 mesh screen was inserted, along with an expanding mandrel having a thermal expansion rate greater than that of Incoloy 800. The recommended procedure is to vacuum-fire the assembly to sinter the wick to the pipe wall. This was not done with the first element, and hot spots developed between the wick and outer wall, as discussed in Sec. 3.3.

Following completion of the first wick layer, the next step was to place artery mandrels and 2-1/2 wraps of 100 mesh Type 304 stainless steel (SS) screen on a nylon mandrel and insert the assembly into the heat pipe. Then the nylon mandrel was removed and a rubber balloon hose was inserted and

HEAT PIPE ELEMENT	DIMENSION			PIPE BODY	WORKING FLUID	WICK STRUCTURE
	A	B	C			
70 cm units	3' - 4-3/4"	0' - 9"	2' - 7-3/4"	2" IPS Sch. 10 Incoloy 800	80 g Sodium	One wrap of 100 mesh SS screen sintered to wall, followed by two additional wraps of screen with two 0.125" ID arteries.
Full scale 4 m unit	13' - 3-3/4"	6' - 0"	7' - 3-3/4"	2" IPS Sch. 10 Incoloy 800	450 g Sodium	Knurled at 50/in. along Dim. "B" length, followed by two continuous wraps of 100 mesh SS screen with two 0.125" ID arteries.

Note: The fill tube assembly and protective enclosure shown are typical of the full scale prototype only.

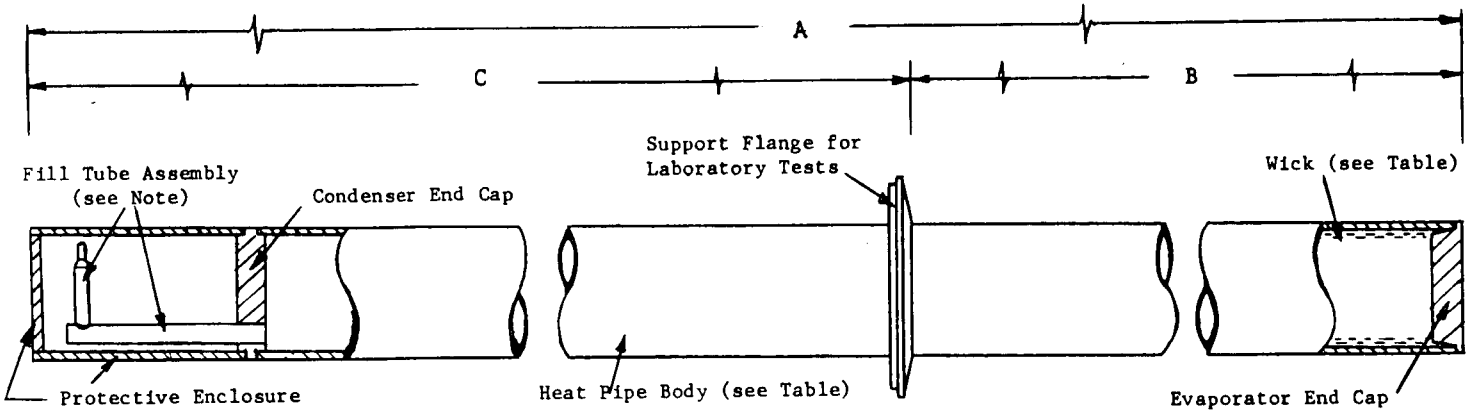

Fig. 3. Design Layout for Prototype Heat Pipe Assemblies

pressurized to better form the arteries and to press the secondary wick layers into place. Following removal of the hose and artery mandrels, the evaporator end of each artery was pinched shut, and the heat pipe end caps were welded in place.

The assembly was next purged in a glove box with argon and 80 g of sodium added through a small fill tube (see Fig. 3). The heat pipes were pumped down to a vacuum of $\sim 10^{-6}$ torr, then sealed by fusion closure of the fill tube.

The final fabrication step involved the application of protective surface coatings for erosion, corrosion, and hydrogen permeation barriers. This involved a plasma spray coating of Fecraly, followed by a layer of magnesium-zirconate cladding. The coatings were applied to the evaporator or in-bed section only.

3.3 LABORATORY ACCEPTANCE TESTS

The prototype heat pipes were all made of 2 in. Schedule 10 Incoloy 800 pipe (6.03 cm OD, 0.34 cm wall) and a screen/artery wick structure made of 100 mesh Type 304 SS screen. Two arteries 3.18 mm (0.125 in.) OD were used in each heat pipe. Further details of the construction of these heat pipes is provided in Ref. 1.

The first heat pipe was removed from the vacuum system where it had been processed and sealed, and was tested in air using an induction heat source. The first tests were conducted with the heat pipe horizontal. At a power level estimated at 2450 W, the heat pipe operated with an evaporator temperature of 693°C (1280°F) and a ΔT of 12°C (22°F). The power was increased to an estimated 2875 W. Hot spots appeared in the evaporator area between the arteries. The heat pipe ΔT was 14°C (25°F), except for the hot spots, which were about 100°C hotter.

After the test, the heat pipe was plasma-spray-coated with protective layers of Fecraly and magnesium-zirconate. Then it was subjected to a flame heated life test at a nominal temperature of 871°C (1600°F). During this test there was no further evidence of the presence of gas, which would have caused a cold condenser end. There were seven on-off thermal cycles during this life test, yet there was no evidence of degradation of the temperature profile, as had occurred during an earlier heat pipe life test [1]. It was concluded that the Fecraly/magnesium-zirconate coating was effective in suppressing hydrogen permeation and preventing scratching of the permeation-resistant layer.

Eventually, the heat pipe failed due to a sodium leak at the condenser end and the test was stopped. When the heat pipe was removed from the test furnace, it was observed that a blister had developed in the magnesium-zirconate coating in the area of flame impingement. The underlying Fecraly was oxidized, but appeared to be intact and well bonded to the heat pipe. The blister was most likely caused by the hot spots observed in the preliminary testing of this heat pipe.

The area of sodium leak was x-rayed but the cause was not determined. In subsequent discussions with Huntington Alloys personnel, it was learned that there is evidence that cracking has occurred when 308 SS filler rod is used

with Incoloy 800. This was the process weld material used in the failed heat pipe, and probably was the cause of the sodium leak. Inconel Filler Metal #82 weld rod was used for the second heat pipe.

The second Incoloy 800 heat pipe was removed from the vacuum system after sealing, and tested in air in the horizontal position. The ΔT was 14°C (25°F) at an evaporator temperature of 693°C (1280°F) and a power estimated at 2430 W. The heat pipe evaporator was elevated 6.5° against gravity and the power increased to an estimated 3840 W. Under continued testing, a power of 7900 W was reached at 835°C (1535°F) with a ΔT of 28°C (50°F). No hot spots were observed at any time during these tests, demonstrating the value of sinter-bonding of the wick to the evaporator wall. This heat pipe was coated with Fecraly and magnesium-zirconate and delivered to ANL. This second heat pipe was used in the Heat Pipe Test Facility to obtain heat pipe performance data.

4. HEAT PIPE TEST RESULTS

The coupling of the condenser section of the heat pipe and the gas-water calorimeter was the method employed in the experiment to control the overall heat transfer through the heat pipe. Tight coupling was obtained by having gas present in the calorimater gap to enhance the heat transfer from the heat pipe to the calorimeter. This allowed for combined radiation, conduction, and convection in the calorimeter gas gap. A loose coupling was obtained by having the calorimeter gap evacuated, making thermal radiation the only mode of heat transfer between the condenser section of the heat pipe and the calorimeter.

The series of events during the test program can be summarized as follows:

1. High-power tests using a tightly coupled calorimeter
2. Failure and removal of the Fecraly/magnesium-zirconate coating
3. Low-power tests using a loosely coupled calorimeter
4. Heat pipe failure
5. Post-test examination of the failed heat pipe

Table 1 contains the steady-state heat pipe data obtained with a tightly coupled calorimeter. These data were obtained by setting a fixed power level and fixed calorimeter flow and allowing the evaporator temperature to reach equilibrium. The power throughput during steady-state operation was obtained by an energy balance on the calorimeter. These data are discussed in Sec. 5.

After obtaining the data presented in Table 1, flaking of the Fecraly/magnesium-zirconate coating was observed on the surface of the evaporator section. A hot spot was evident in the same general area where the flaking was occurring. It was felt that this hot spot was occurring because of the coating--the coating either was of a nonuniform thickness or was separating from the pipe wall. The coating was removed by machining to allow additional heat pipe testing. The examination and removal of the Fecraly/magnesium-zirconate coating are described in Sec. 6.

Removal of the Fecraly/magnesium-zirconate coating allowed heat pipe testing to continue. The hot spot on the heat pipe remained after coating removal, although the temperature at the hot spot was significantly reduced.

Additional heat pipe testing was conducted using a loose coupling with the calorimeter. The gas was evacuated so that thermal radiation was the only mode of heat transfer between the condenser section of the heat pipe and the calorimeter. The data were gathered in two sets; the second set was taken several months after the first set to verify heat pipe performance. These data are shown in Table 2, and are discussed in Sec. 5.

Startup and operation of the heat pipe several months after the taking of the data in Table 2 resulted in a pinhole leak in the evaporator section of

Table 1. Steady-state Heat Pipe Data

Evaporator Temperature, °F	Calorimeter Flow, gpm	Calorimeter ΔT, °C	Power Throughput, kW
1418	2.0	13.0	6.86
1605	2.0	15.9	8.39
1550	3.0	9.95	7.87
1520	3.0	9.37	7.42
1565	4.0	7.80	8.23
1555	4.0	7.72	8.15
1540	4.0	7.51	7.92
1505	4.0	6.94	7.32
1485	4.0	6.66	7.03
1475	2.0	12.34	6.51
1407	2.0	12.68	6.69
1430	2.0	13.20	6.96
1448	2.0	13.38	7.06
1480	4.0	7.25	7.65
1535	4.0	7.38	7.79
1525	4.0	7.38	7.79
1552	4.0	7.54	7.96
1580	4.0	7.83	8.26
1570	4.0	7.58	8.00

Table 2. Steady-state Data from Heat Pipe with Coating Removed

Evaporator Temperature (°F)	Calorimeter Flow (gpm)	Calorimeter ΔT (°C)	Power (kW)
	First Set		
1358	2.0	4.13	2.18
1415	2.0	4.17	2.20
1430	2 0	4.05	2.14
1465	2.0	4.49	2.37
1520	2.0	5.20	2.75
1558	2.0	5.81	3.07
1595	2.0	6.45	3.41
1590	2.0	6.45	3.41
1598	2.0	6.70	3.54
1547	2.0	5.77	3.05
1493	2.0	4.97	2.62
1447	2.0	4.35	2.30
1376	2.0	3.80	2.01
	Second Set		
1304	2.0	3.28	1.73
1496	2.0	4.66	2.46
1536	2.0	5.43	2.87
1572	2.0	6.15	3.25
1478	2.0	4.90	2.59
1358	2.0	3.70	1.95

the heat pipe in the region of the hot spot. Since the heat pipe was being operated at less than one atmosphere, air entered the heat pipe through the pinhole leak and the sodium air reaction was contained within the heat pipe. The post-test examination of the heat pipe is described in Sec. 7.

5. DISCUSSION OF EXPERIMENT RESULTS

5.1 COMPARISON OF EXPERIMENT DATA AND ANALYTICAL RESULTS—HEAT PIPE WITH TIGHTLY COUPLED CALORIMETER

Table 1 lists experiment data for the heat pipe operating in the range 1400-1600°F, with heat transport rates in the range 6.51-8.39 kW. The heat pipe geometry was modeled by the heat pipe analysis code ANL/HTP, which is described in Refs. 1 and 2. Calculations were run to evaluate the pipe performance and operating states.

Figure 4 shows the data from Table 1 as open diamond shapes and the results of the ANL/HTP computer calculations as a solid line, with values calculated every 10°C. Appendix A is a listing of the computer output for this case, including the heat transport, the temperature drops through the pipe wall/wick, and the vapor temperatures at the beginning of the evaporator and at the end of the condenser. Also listed are the calculated heat-transport limits for the various temperatures.

As shown in Fig. 4, the experimental data display a nearly linear variation with evaporator temperature, suggesting nearly constant thermal resistance from the evaporator wall to the calorimeter. The slope of a line passed through these data approximates the total thermal conductance, and was used to evaluate the heat transfer coefficient between the condenser wall and the calorimeter. From the data shown in Fig. 4, and accounting for the thermal resistances of the pipe walls, this heat transfer coefficient was calculated to be 94 Btu/hr-ft^2-F. This high heat transfer coefficient was caused by the presence of vacuum pump oil being trapped in the calorimeter.

The analytical results shown in Fig. 4 agree well with the measured data. The values listed in the computer output (Appendix A) indicate that the pipe operation was normal, with the vapor nearly isothermal, and the pipe operating well below the calculated performance limits.

5.2 COMPARISON OF EXPERIMENT DATA AND ANALYTICAL RESULTS—HEAT PIPE WITH LOOSELY COUPLED CALORIMETER

Table 2 presents measured data for the heat transport vs. evaporator temperature, for two different test sequences. These test sequences were taken on different dates, with the annular gas gap in the calorimeter evacuated to vacuum levels between 2×10^{-4} torr and 8×10^{-4} torr, which varied for different temperatures. For these vacuum levels, gas conduction and gas convection heat transfer can be considered negligible (i.e., loosely coupled to the calorimeter), and the heat transfer mode from the condenser can be considered to be only thermal radiation.

Figures 5 and 6 show these data, along with a least-squares curve, fit to the equation

$$Q = C(T^4 - T_o^4) ,$$

where T is assumed equal to the measured evaporator wall temperature, and T_o is the measured cooling water inlet temperature. The calculated values of C

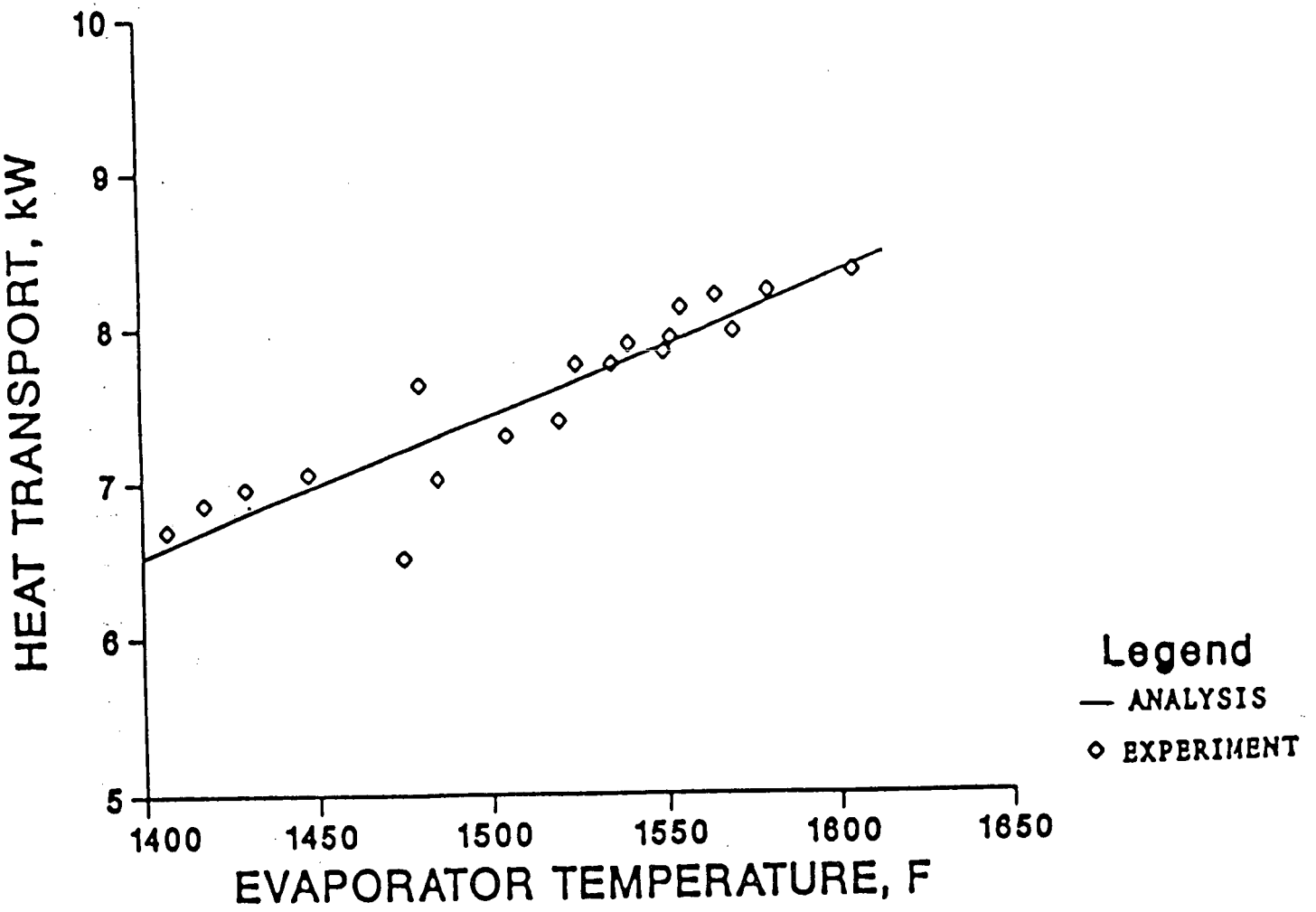

Fig. 4. Heat Transport vs. Evaporator Temperature
(28 in. long 2 in. IPS heat pipe)

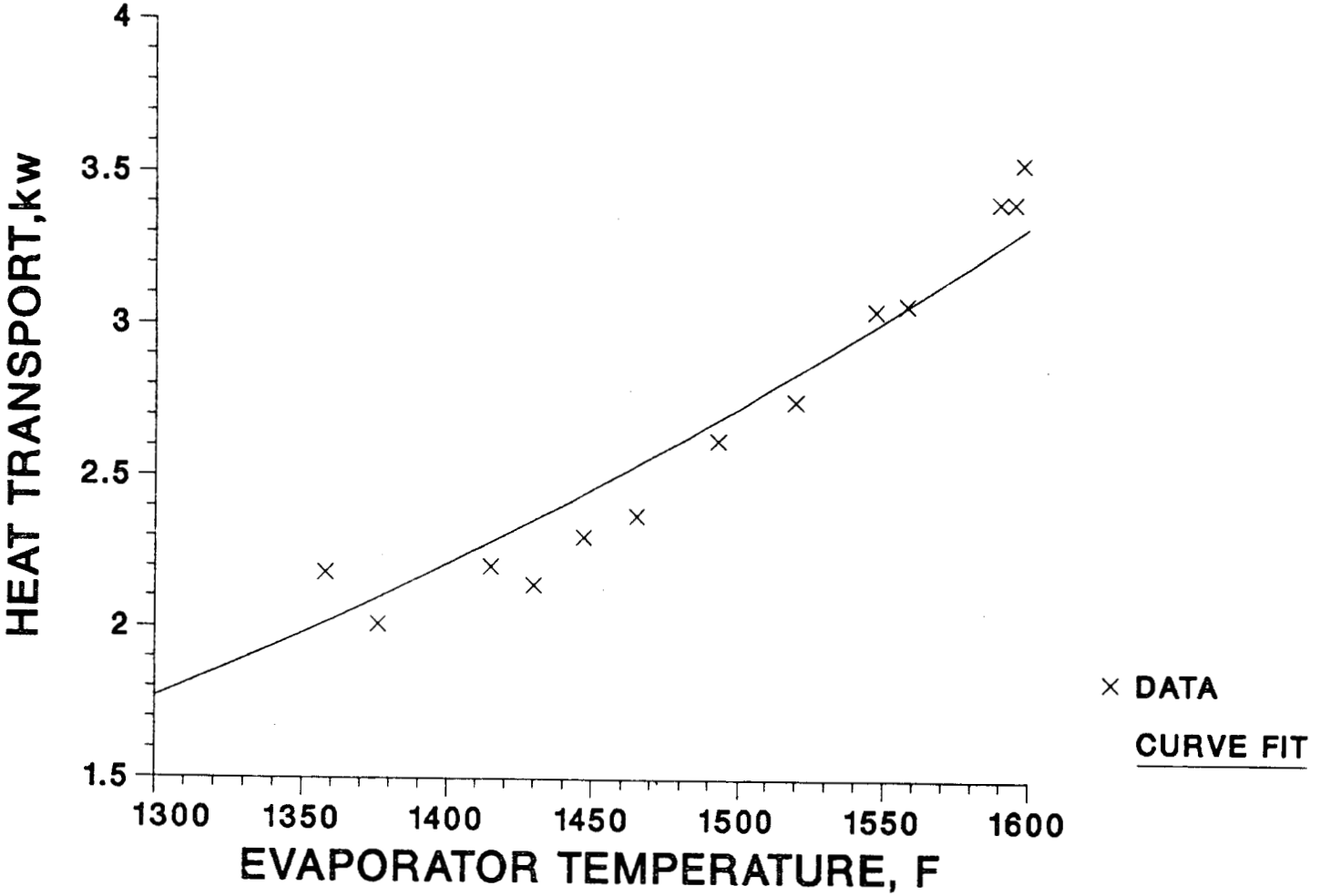

Fig. 5. Comparison of Heat Pipe Experimental Data (from Table 2, First Set) and Calorimeter Radiation Model

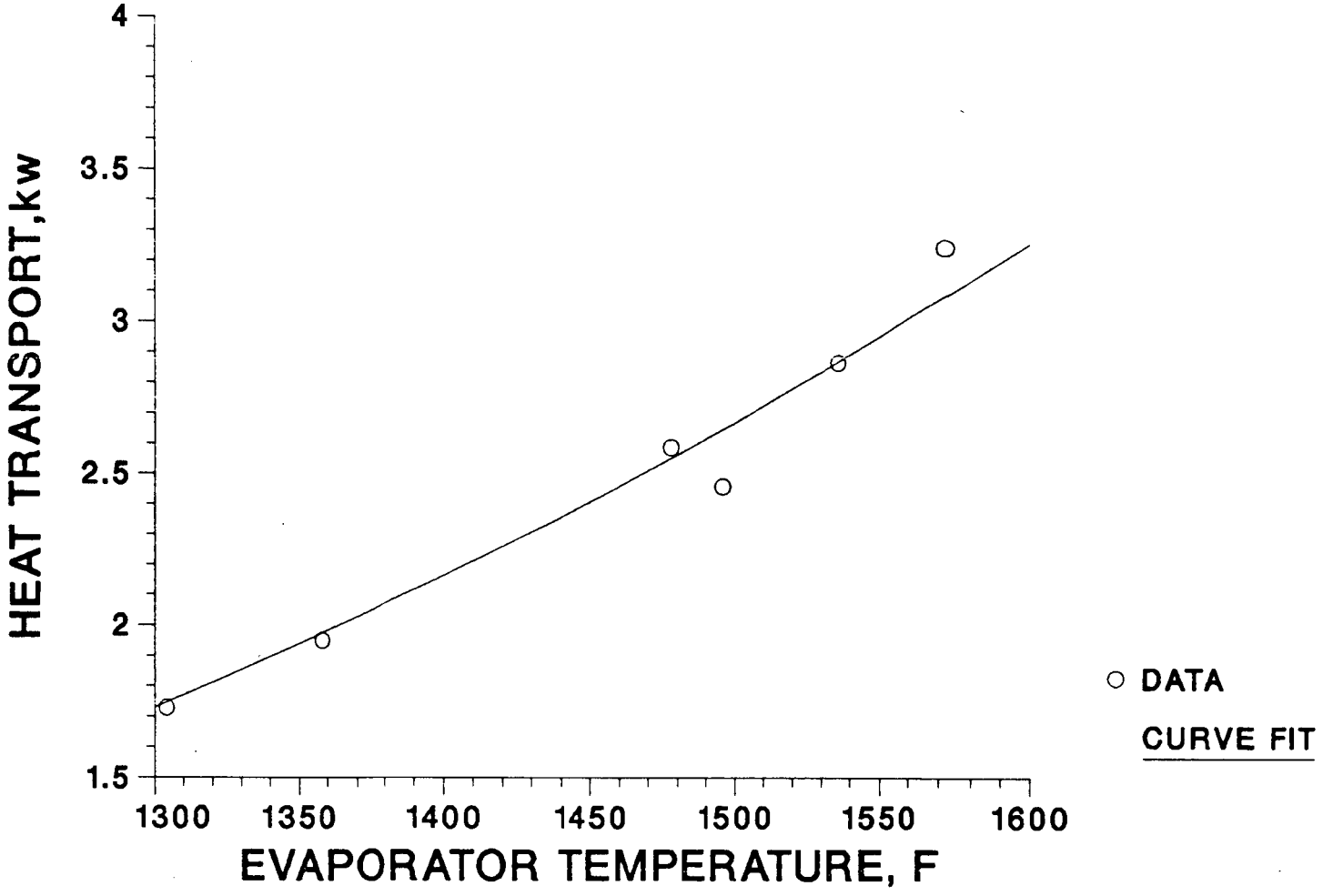

Fig. 6. Comparison of Heat Pipe Experimental Data (from Table 2, Second Set) and Calorimeter Radiation Model

were 1.800×10^{-13} Kw/R^4 and 1.851×10^{-13} Kw/R^4, respectively, for the curves in Figs. 5 and 6. Figure 7 shows a plot of the data from Table 2, and a least-squares curve fit to all the data. For this curve the calculated value of C is 1.834×10^{-13} Kw/R^4.

To evaluate how well these data correlate to radiation heat transfer, it is necessary to compare the experimental values for C against values calculated from a radiation model, using values for the heat transfer area and the overall effective emissivity;

$$Q = C\ (T^4 - T_o^4) = \bar{\varepsilon}\sigma A(T^4 - T_o^4)\ .$$

From this, the effective emissivity is

$$\bar{\varepsilon} = \frac{C}{\sigma A}\ .$$

For the heat pipe mounted in the calorimeter, the length radiating was estimated to be about 18.25 in. With a nominal diameter of 2.375 in. and an end cap and fitting, the radiation area was estimated to be 0.978 ft^2. Using this and an average value of $C = 1.825 \times 10^{-13}$ Kw/R^4, the effective emissivity is

$$\bar{\varepsilon} = \frac{C}{\sigma A} = 0.372\ ,$$

which is not an unrealistic value. Thus, the measured data correlate quite well with a radiation model, using realistic estimates for the surface area and overall effective emissivity, and the calorimeter appears to be operating in a radiation mode, with reproducible results obtained in independent experimental runs.

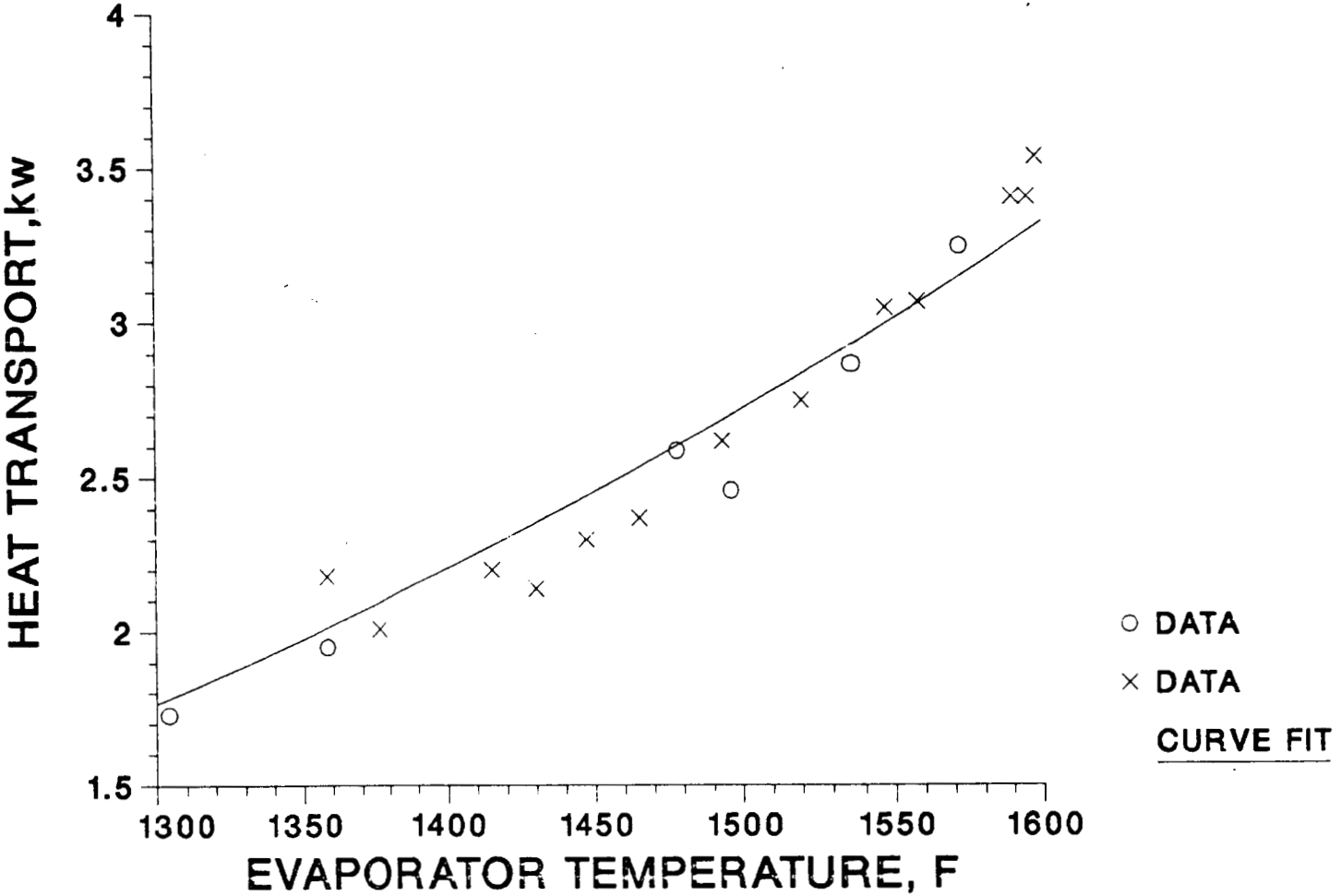

Fig. 7. Comparison of Heat Pipe Experimental Data (Table 2, First and Second Sets) and Calorimeter Radiation Model

6. EXAMINATION OF THE FECRALY/MAGNESIUM-ZIRCONATE COATING

The Fecraly/magnesium-zirconate coating was applied to the 2-3/8 in. OD 28 in. long heat pipe to allow it to withstand hydrogen permeation, as well as the harsh conditions in a fluidized-bed combustor (FBC). In an FBC application, the heat pipe outside wall temperature is fixed by the bed temperature and the inside wall temperature is fixed by the sodium temperature. The heat transfer into the pipe is determined by the thermal resistance of both the heat pipe wall and the protective coating on the outside diameter of the pipe.

In the HPTF, a nearly uniform heat generation rate occurs in the pipe wall; hence, a near uniform heat flux is supplied to the sodium in the evaporator section. Since the inside wall temperature of the evaporator section of the pipe is determined by the sodium temperature, the outside wall temperature of the pipe wall will have a nonuniform temperature as a function of the combined thermal resistance of the heat pipe wall and the Fecraly/magnesium-zirconate coating. This nonuniform temperature was observed during operation; a photograph of this heat pipe during operation is shown in Fig. 8. The hot spot shown on the top of the pipe in Fig. 8 was at the same location on the pipe regardless of the rotation of the pipe in the test apparatus. Hence, it was determined that there existed some difficulty with the coating or that the wick structure was not attached to the inside of the pipe at this location. Flaking of the coating began after additional high-temperature operation of the pipe and it appeared that the nonuniform outside wall temperature was occurring because of coating thickness variation or some other defect in the heat pipe.

Figure 9 illustrates the coating in the area of the hot spot after substantial intermittent operation. Figure 10 shows this same hot spot area from a different angle. Apparently, the large temperature drop across the Fecraly coating caused the coating to begin to separate.

In addition to the hot spot area, Fecraly/magnesium-zirconate cladding problems also occurred in the vicinity of the evaporator end plate. Figure 11 shows an end view of this heat pipe where the coating had flaked off the wall at the end plate weld bead corners. Adjacent to the area where the coating had flaked off, there is a region where the coating had begun to separate farther from the heat pipe material.

Figure 12 is another view of the coating separating from the heat pipe wall at the hot spot. Figure 13 shows this same area of the heat pipe after the loose coating had been manually removed. The balance of the coating in this area is still securely bonded to the heat pipe.

Figure 14 shows the end view of the heat pipe evaporator section. The discolored region on the end of the heat pipe is where the coating had been removed by grinding to measure temperature with an optical pyrometer. The area near the end of the pipe where the coating had flaked off and loosened is evident in this photograph. Figure 15 shows this same area of the heat pipe after the loose coating had been manually removed. The balance of the coating in this area is still securely bonded to the heat pipe.

The areas of the heat pipe where the coating lost its bond to the primary heat pipe material were those where a hot spot occurred during heat pipe operation. This hot spot occurrence is illustrated in Figs. 9, 10, 12, and 13. A hot spot also was observed in the area where the coating loosened near the end of the heat pipe (Fig. 11). It appears that the loosening and flaking of the coating material from the heat pipe is due primarily to thermal expansion. Apparently, variation in the coating thickness was the primary candidate reason for the initial occurrence of the hot spots.

Removal and inspection of the coating was initiated to determine variations in coating thickness. Inspection of Figs. 11, 14, and 15 shows that there was a buildup of the coating material in the cylindrical region of the evaporator at the end of the heat pipe. This is a cause for the occurrence of the hot spot. Also, there is the possibility that edge effects make this region more susceptible to flaking and cracking.

The hot spot on the cylindrical surface of the coating was examined by machining off a portion of the Fecraly/magnesium-zirconate coating, as shown in Fig. 16. The results show that the pipe was out of round, the lathe having machined off most of the coating except in that region where the hot spot occurred. It is also apparent that there was a surface defect (i.e., indentation in the Incoloy 800 pipe wall) on the heat pipe in the region where the hot spot occurred. Both these factors appear to have contributed to the excessive thickness of the coating in the region of the hot spot. Figure 17 illustrates the other side of the evaporator section of the heat pipe after this machining took place. The portion of the heat pipe reflecting the most light is where the most material was removed, while the darker region shows part of the existing bond between the coating and the primary heat pipe material.

It appears that the bond between the coating material and the primary heat pipe material was very good over the entire continuous surface of the heat pipe. Even in the area of the hot spot (Fig. 16), the bond between the primary heat pipe and coating appears to have remained strong. The coating apparently was destroyed due to its localized excess thickness, which resulted in large temperature gradients across the coating and excessive thermal stresses. Figure 18 is an additional photograph showing the surface defects that resulted in the hot spot in the Fecraly/magnesium-zirconate coating.

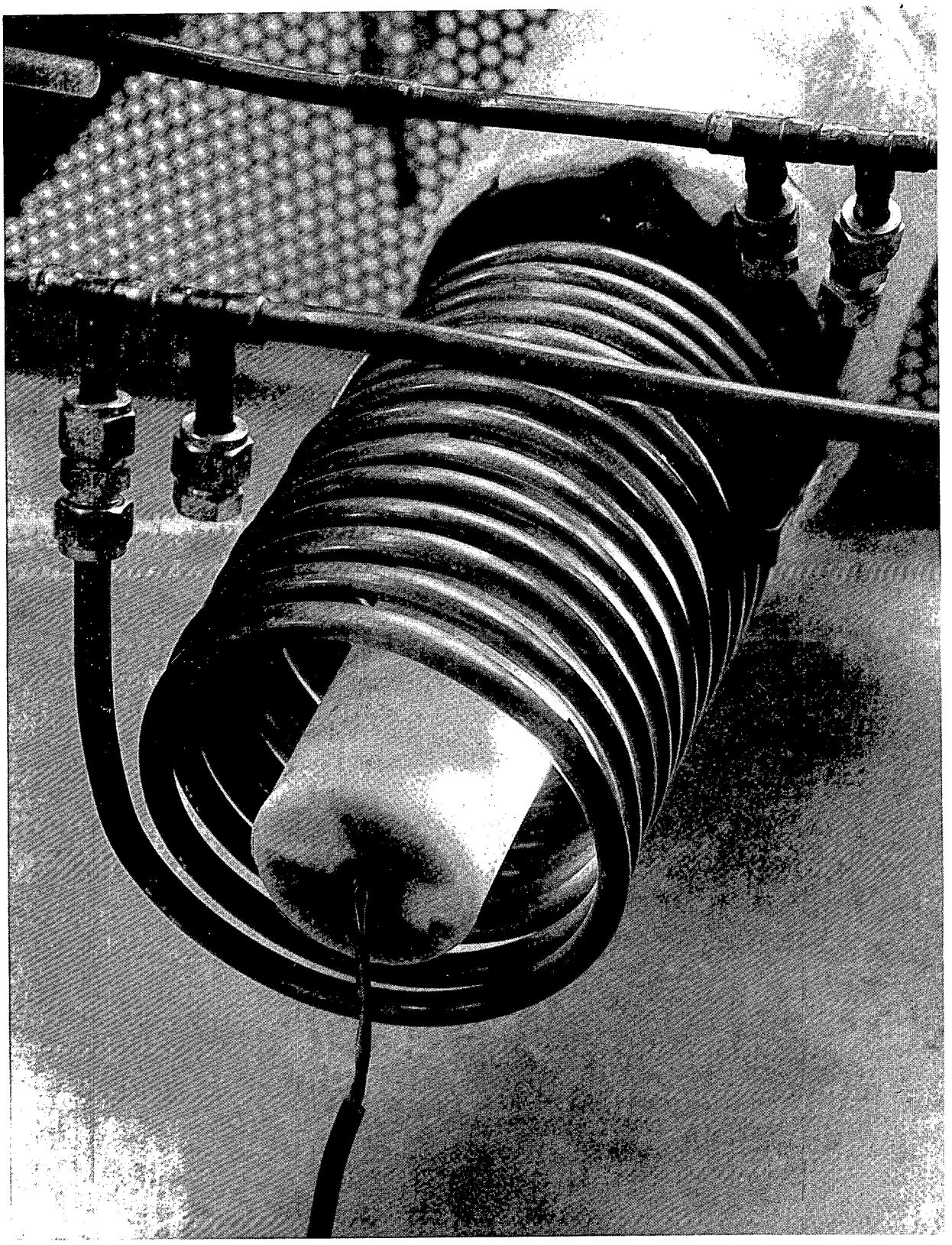

Fig. 8. View of Heat Pipe During Operation.
ANL Neg. No. 113-84-84.

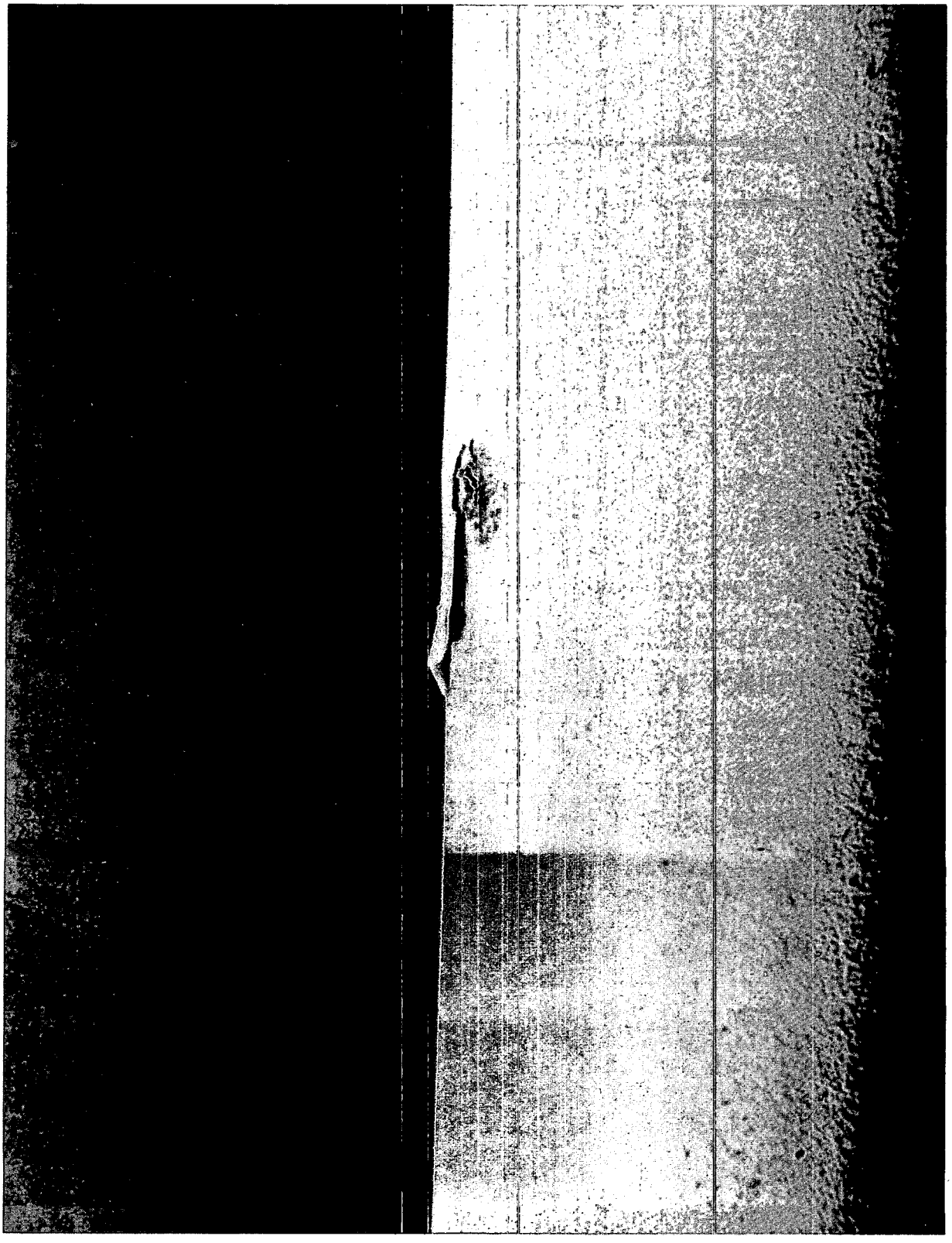

Fig. 9. View of Coating in Area of Hot Spot

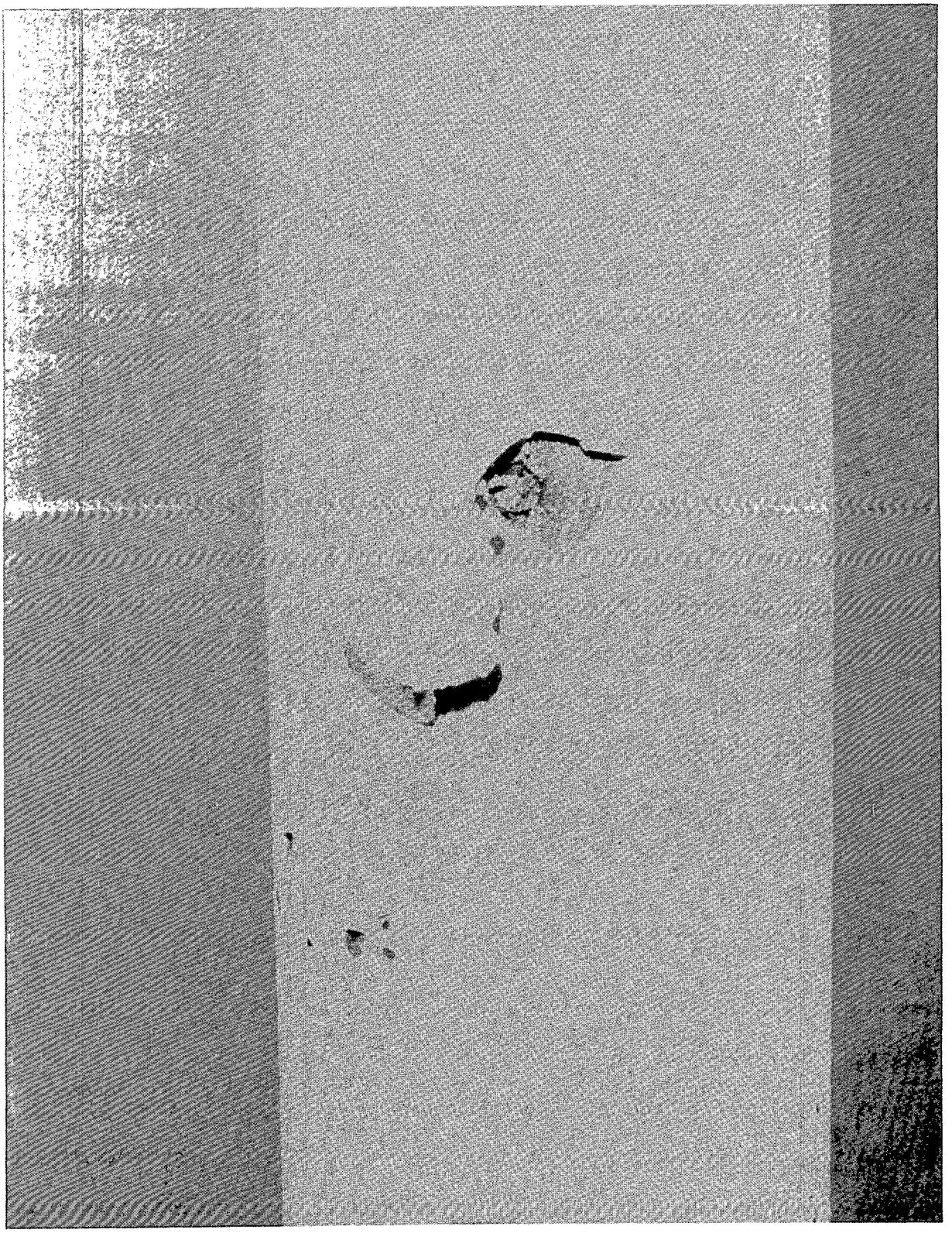

Fig. 10. View of Hot Spot Area from a Different Angle

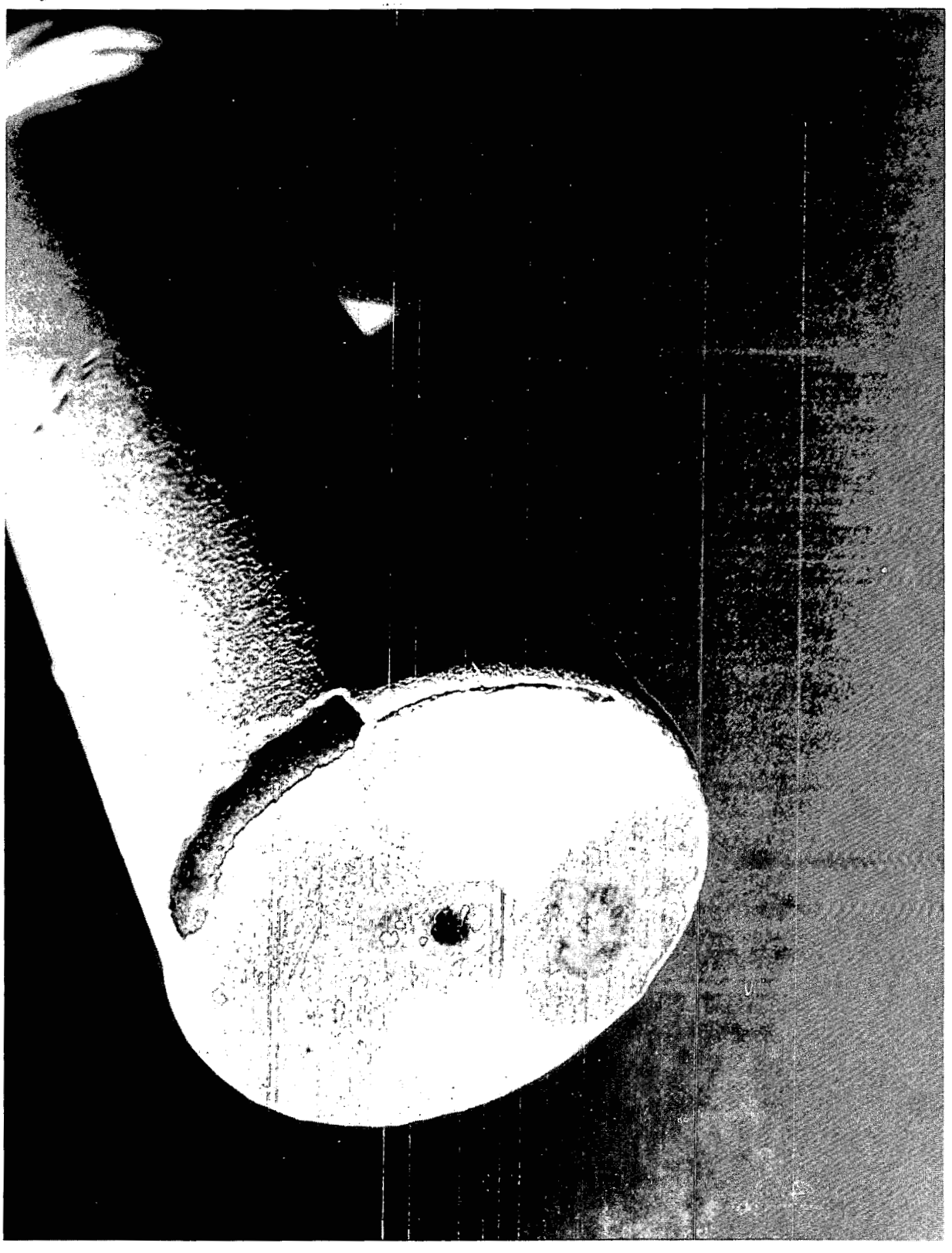

Fig. 11. End View of Heat Pipe where Coating Has Flaked

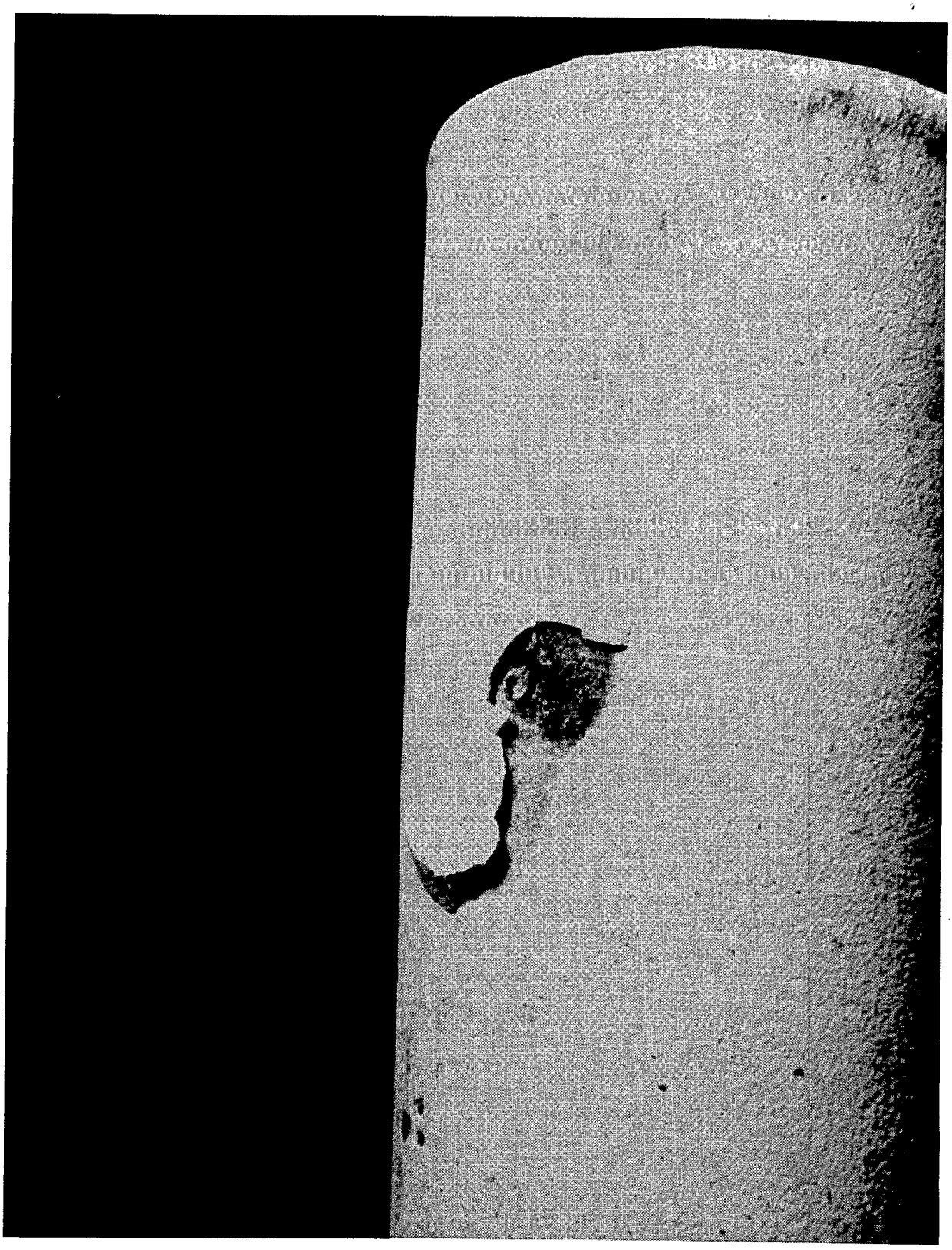

Fig. 12. View of Coating Separating from Heat Pipe at Hot Spot

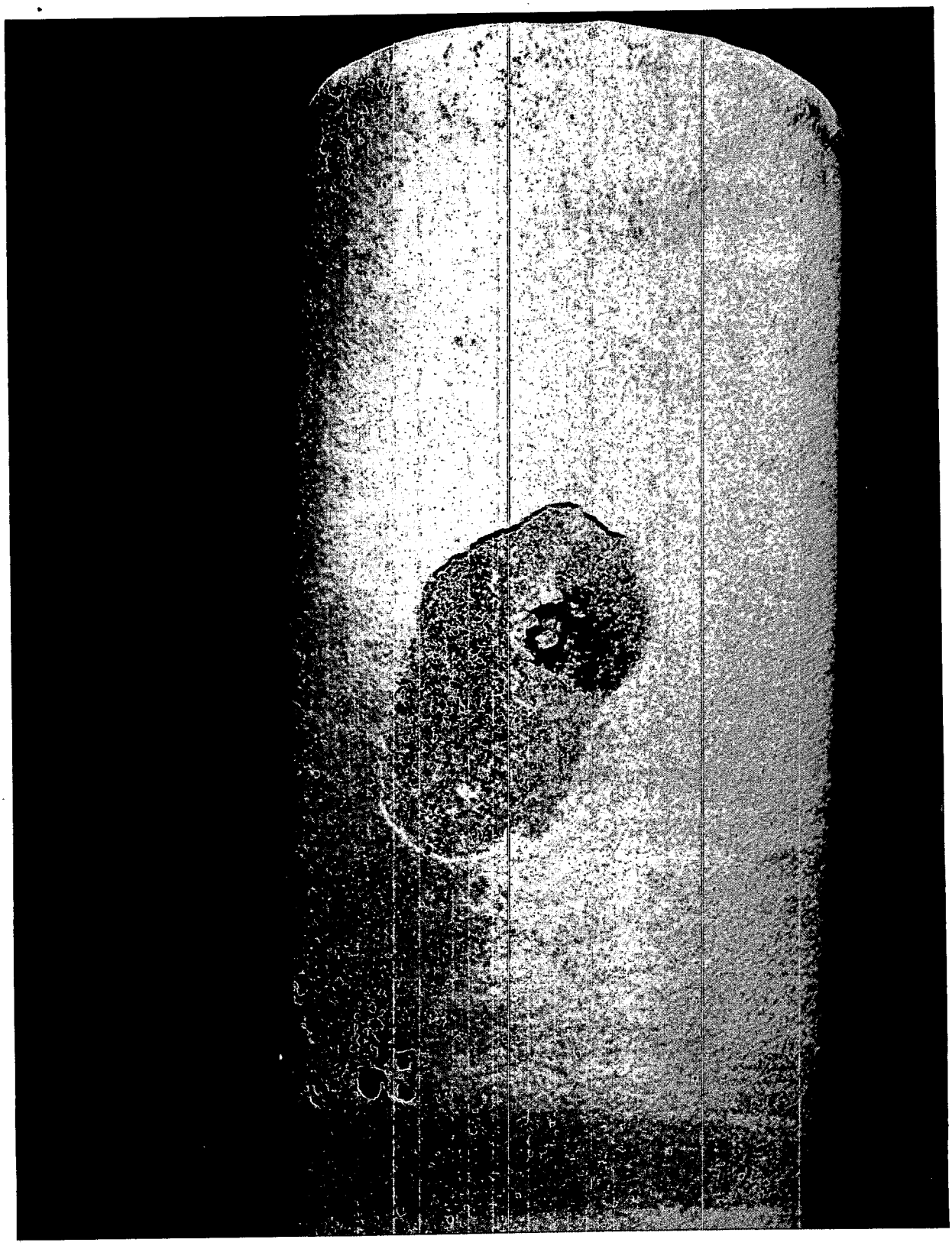

Fig. 13. View of Coating Separating from Heat Pipe after Loose Coating Manually Removed

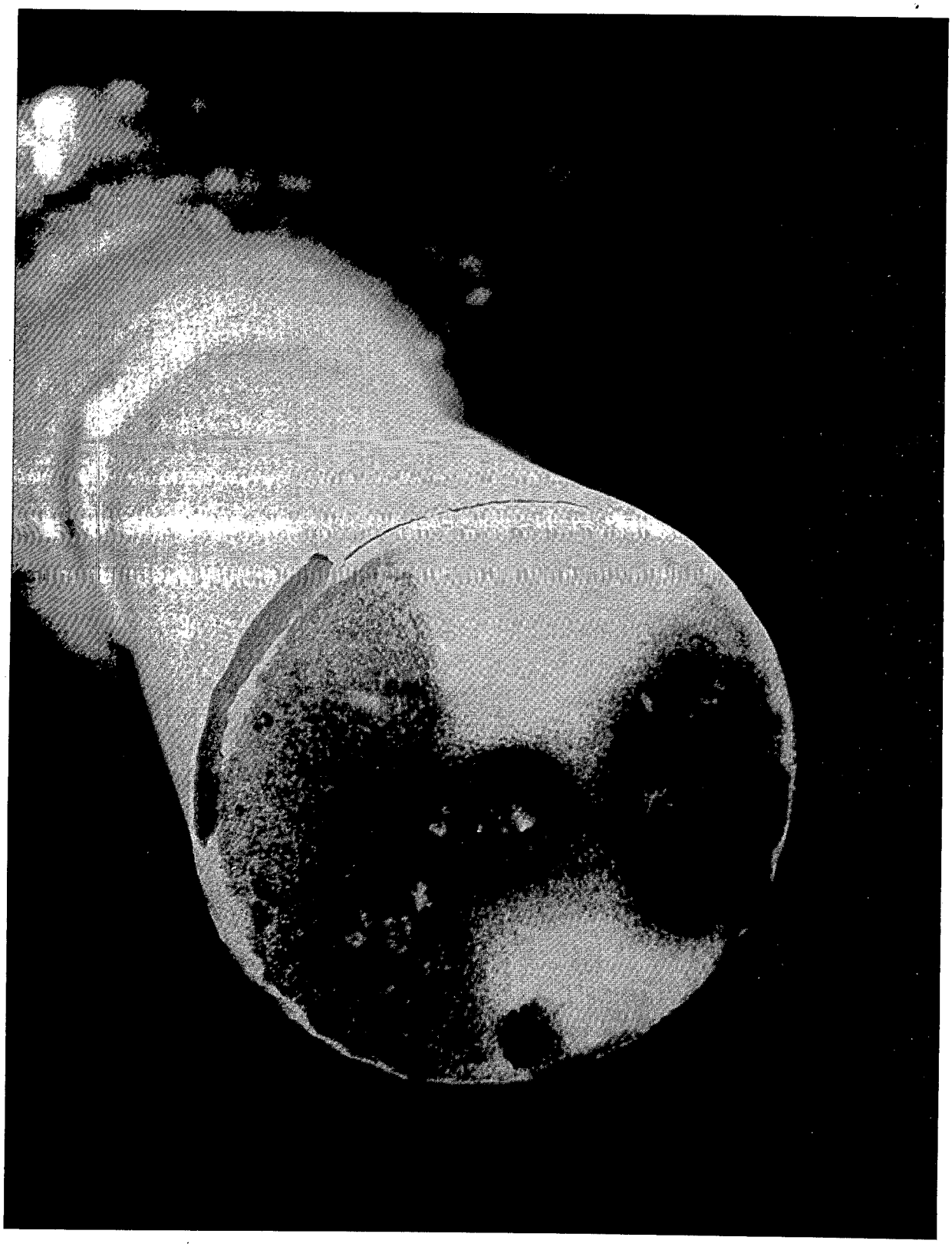

Fig. 14. End View of Heat Pipe Evaporator Section

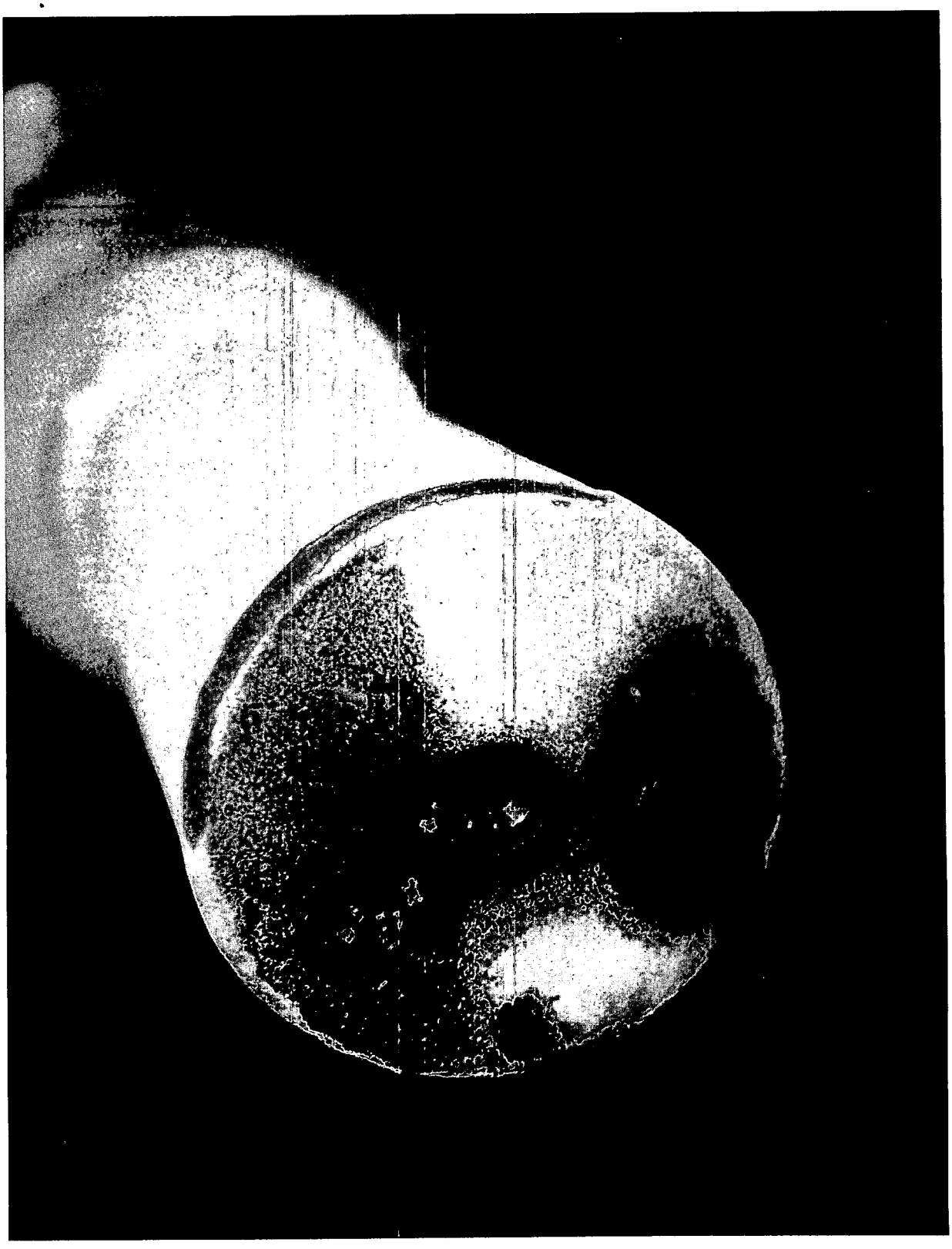

Fig. 15. End View of Heat Pipe after Loose Coating Manually Removed

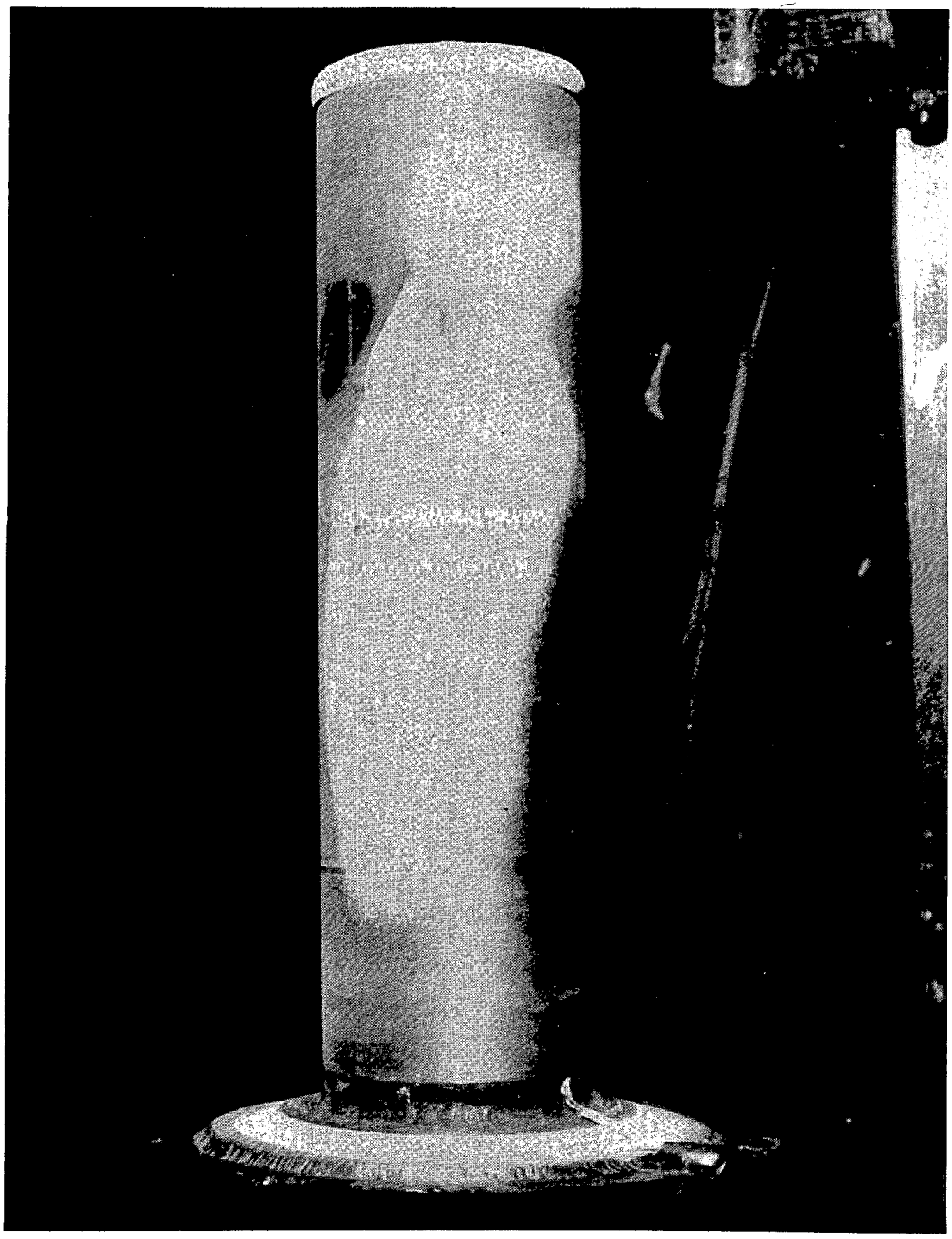

Fig. 16. View of Machined Off Portion of Coating

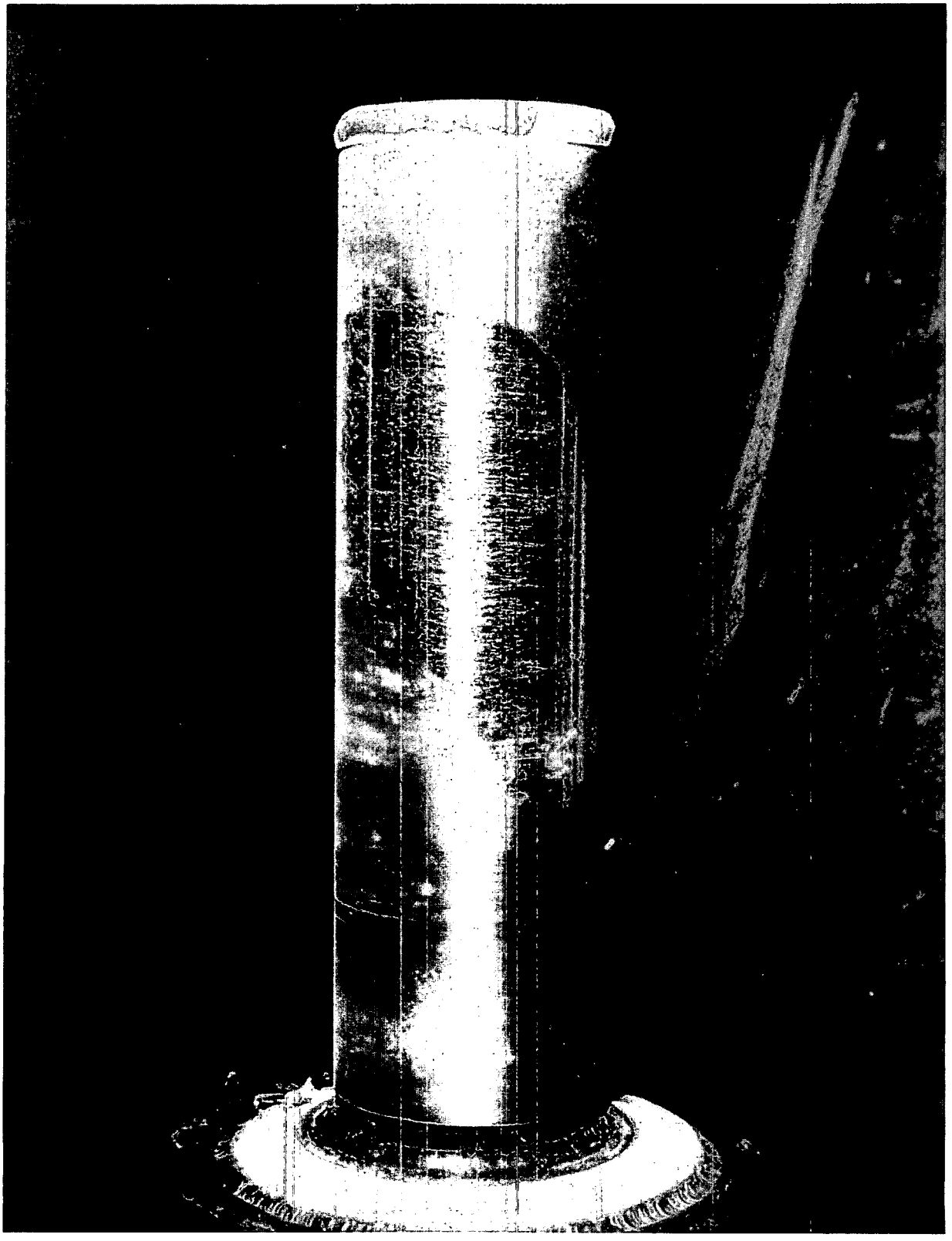

Fig. 17. View of Heat Pipe Evaporator Section after Machining

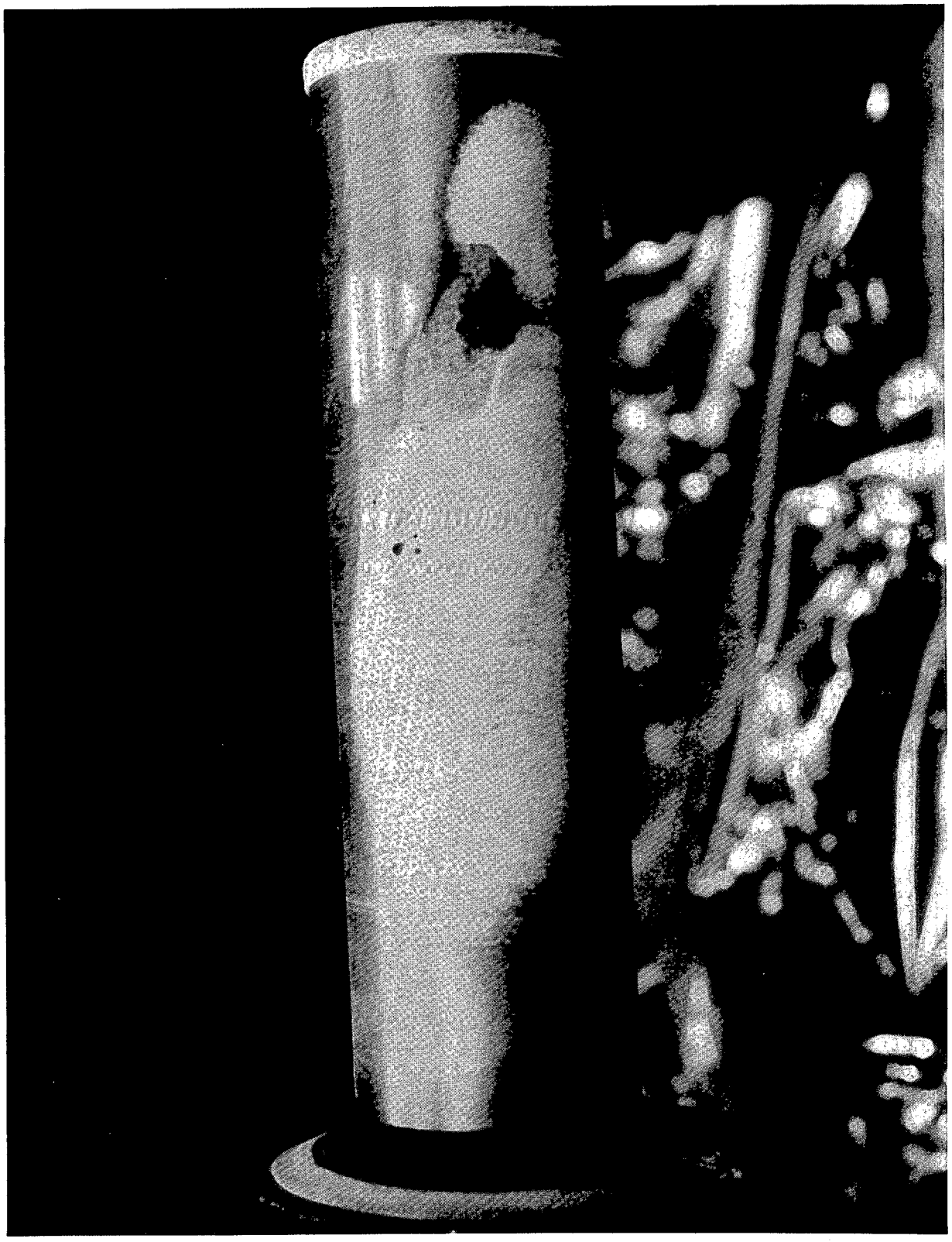

Fig. 18. View of Heat Pipe Defects Resulting from Hot Spot

7. POST-TEST HEAT PIPE EXAMINATION

After the pinhole leak occurred in the evaporator section of the heat pipe, a post-test examination was conducted to attempt to find the reasons contributing to the failure of the heat pipe. This post-test examination involved cutting the heat pipe into sections and photographing the outside, wall, and inside of the heat pipe.

An inspection of the heat pipe internals showed that the wick structure of the pipe remained in its initial configuration, and that at shutdown the sodium working fluid was contained totally within the wick structure of the heat pipe.

Figure 19 shows the outside of the heat pipe before the pipe was cut apart. The surface flaw discussed in Sec. 6 is evident in this photograph. Some of the discolorization in the area of the pinhole leak is sodium oxide.

Figure 20 is an end view of the cut heat pipe, illustrating the location of the pinhole leak, and showing the sodium working fluid contained in the wick structure. Figure 21 shows a similar photograph, taken at a slightly different angle, illustrating the wick structure in place.

After removal of the sodium and the internal wicking, it was observed that melting of the pipe wall had occurred in the region around the hot spot and pinhole leak (Fig. 22). The postulated reason for the hot spot and resultant pinhole failure of the heat pipe was that the pipe was out of round and had an observable defect on the outside wall. This resulted in an excess thickness of coating at this defect location, which resulted in a locally large resistance to heat transfer. In addition, because the pipe was out of round, there was considerable variation in wall thickness. The wall thickness at the hot spot was approximately 0.040 in. thicker than the wall 180° around the perimeter. These factors produced a noticeable hot spot in the heat pipe (visible during pipe operation), which produced axial thermal stresses in excess of the yield stress. The resulting thermal cycling of the heat pipe caused this flaw to propagate into the wall of the pipe, culminating in a leak. Finally, the reaction between the sodium and moist air that entered the heat pipe resulted in a sufficient heat generation rate on the inside surface of the pipe to melt some of the inside surface and do significant local damage to the pipe wick structure. Figure 23 shows the melting that occurred on the inside of the heat pipe during the reaction between the sodium working fluid and the moist air that entered the pipe through the pinhole leak.

Fig. 19. Evaporator End of Heat Pipe Prior to Post-Test Examination

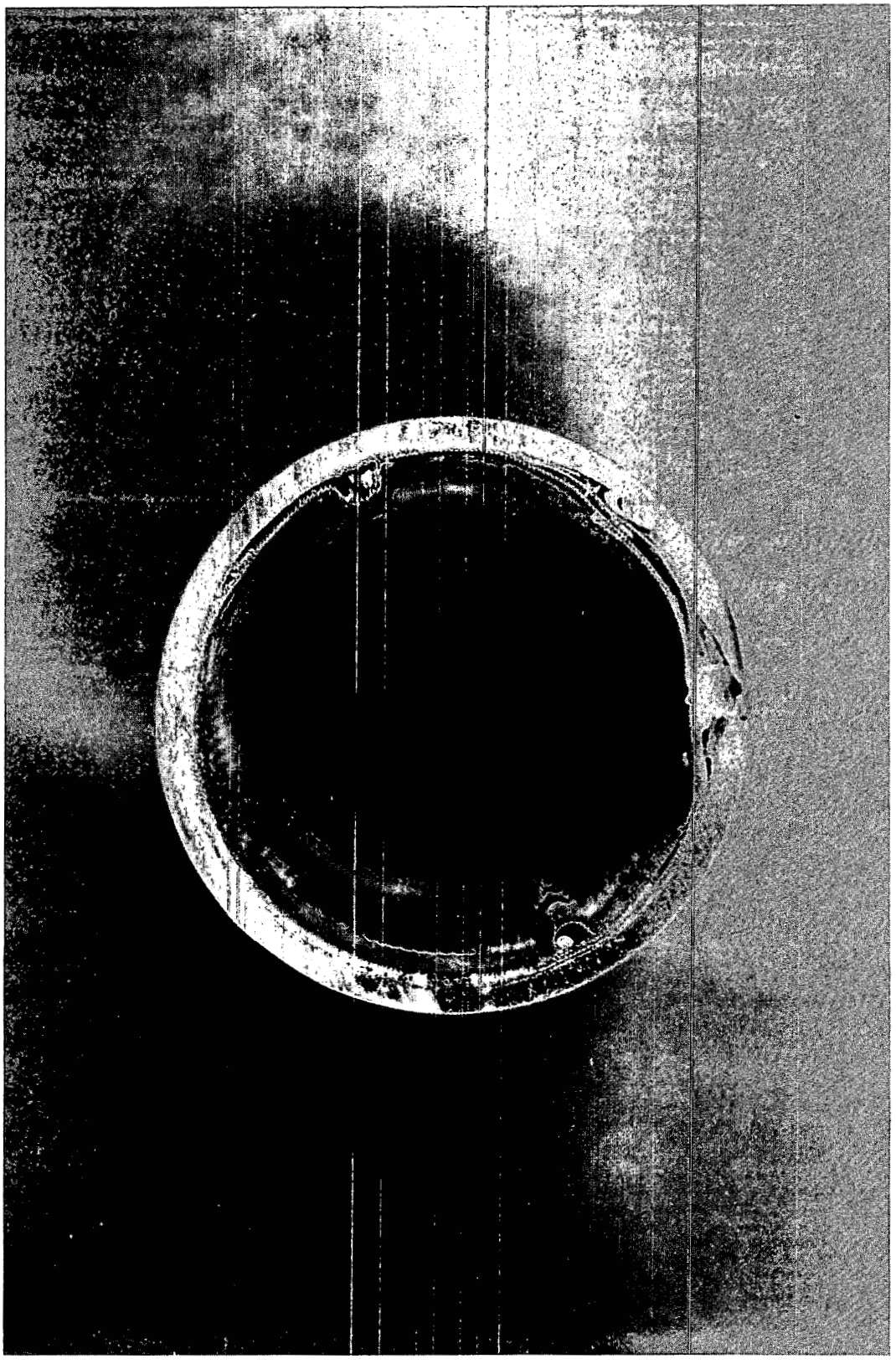

Fig. 20. End View of Evaporation Section of Cut Heat Pipe

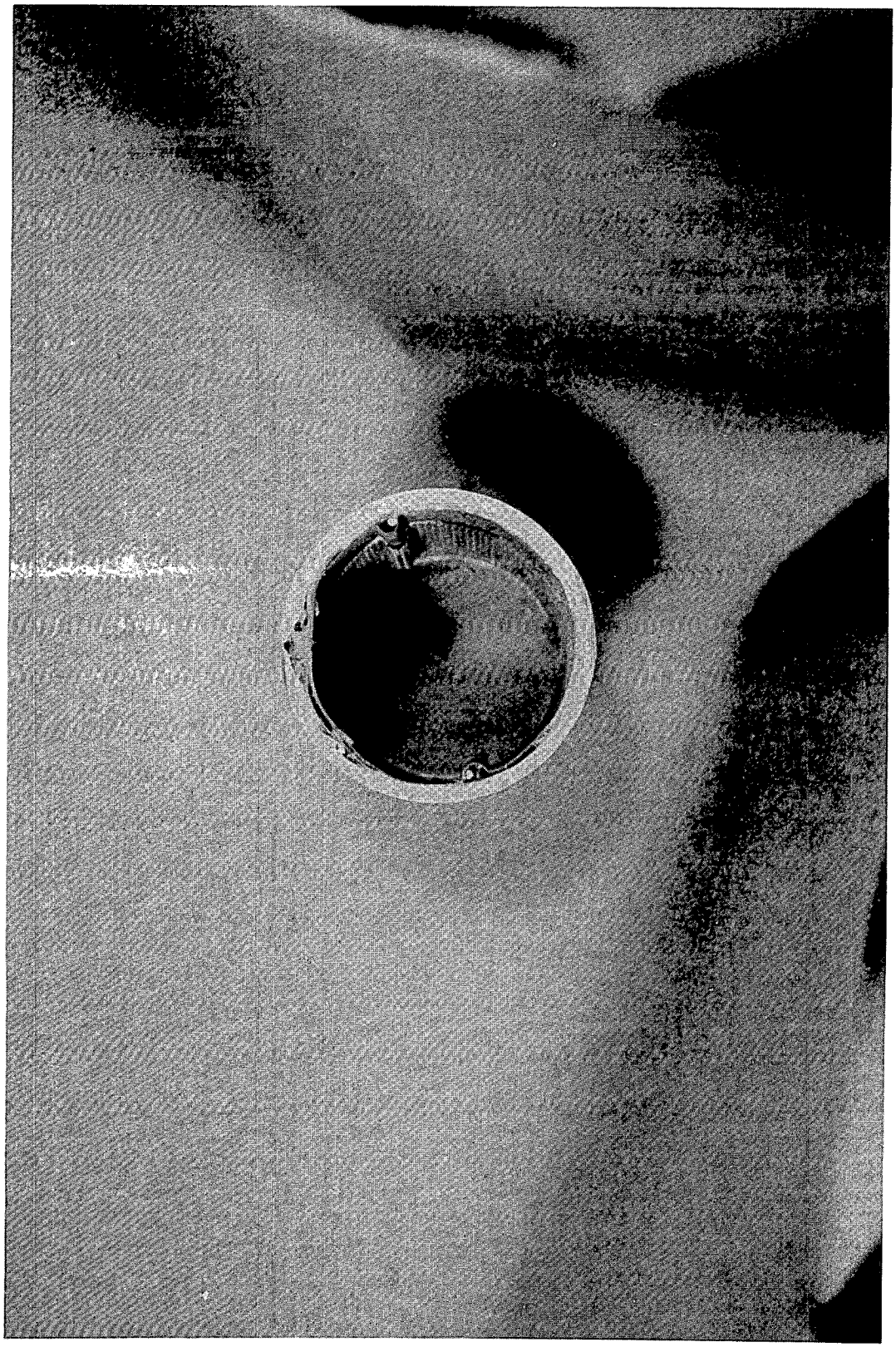

Fig. 21. End View of Evaporation Section of Cut Heat Pipe (different angle)

Fig. 22. Heat Pipe Cross-sections and Internal Wall Showing Melting of Inside Wall

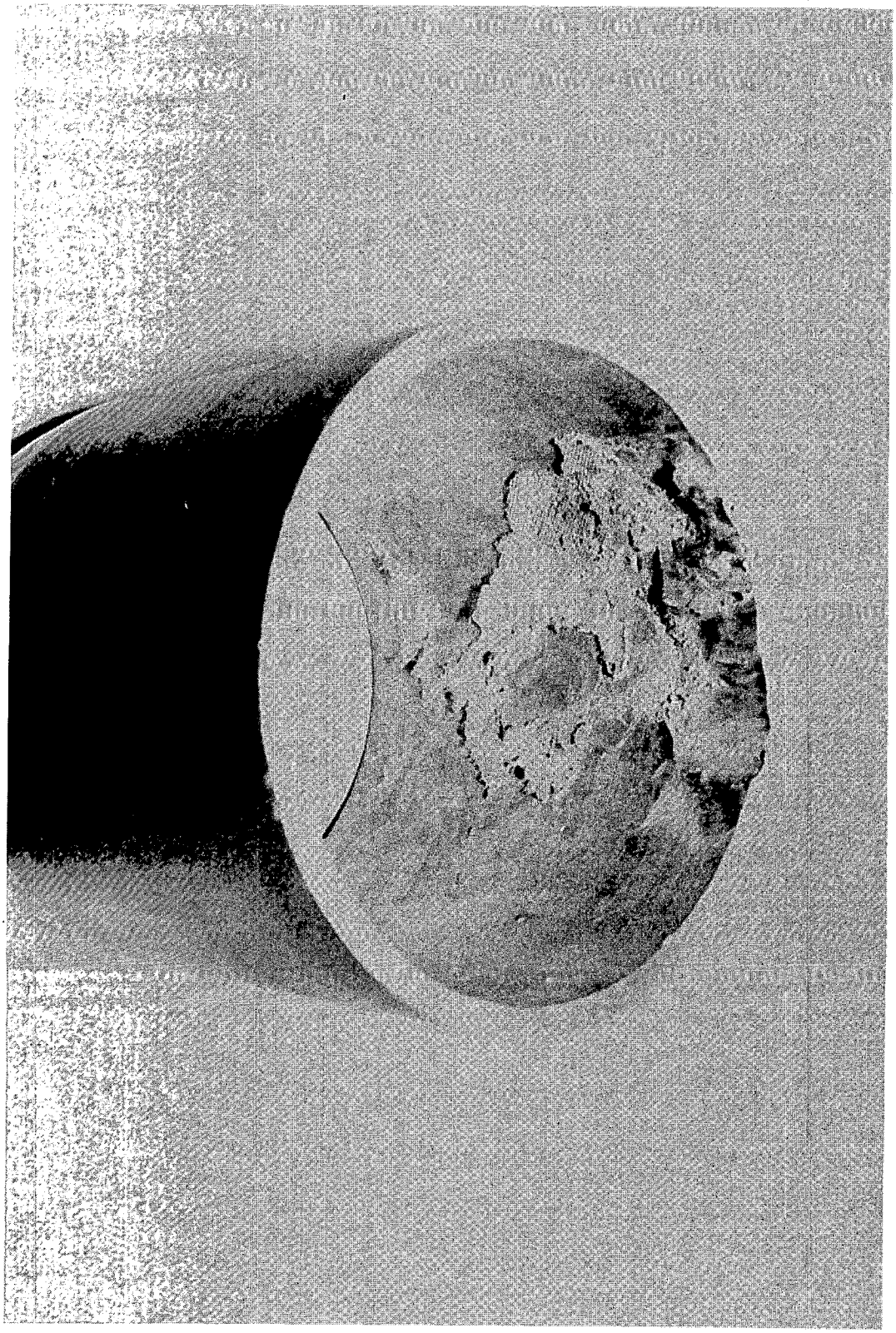

Fig. 23. Heat Pipe Internal Wall Showing Melting of Inside Wall

8. SUMMARY AND CONCLUSIONS

The operation of a prototype heat pipe in the Heat Pipe Test Facility (HPTF) has provided experimental data with both a tightly coupled and a loosely coupled calorimeter. The tightly coupled calorimeter results are similar to those that would be experienced in a fluidized-bed combustor application, and the loosely coupled calorimeter results are prototypic of those that would be experienced in a space environment. The experiment results show good agreement with the heat pipe analytical model [2]. Over a substantial period of operation and over much thermal cycling, the heat transfer performance of the heat pipe proved reliable. Additional testing of longer heat pipes under controlled laboratory conditions will be necessary to determine performance limitations and to complete the design code validation.

The failure of the Fecraly/magnesium-zirconate coating can be attributed to a substantial flaw in the primary containment of the heat pipe and the test conditions of the experiment. However, the evaluation of plasma-spray coating techniques, and possible development of improved coating techniques and materials for FBC application, should be pursued.

Since these tests were on a prototype heat pipe that was built to establish the techniques to fabricate long, high-temperature heat pipes, no real quality control of the heat pipe materials or fabrication procedures were specified. The eventual failure of the heat pipe due to a flaw in the primary containment pipe is an indication that an appropriate level of quality control will be necessary to assure reliable operation of heat pipes.

In the HPTF, a nearly uniform heat generation rate occurred in the pipe wall; hence, a near-uniform heat flux was supplied to the sodium in the evaporator section. Since the inside wall temperature of the evaporator section of the pipe was determined by the sodium temperature, the outside wall temperature of the pipe wall had a nonuniform temperature due to variations in thermal resistance. The temperature nonuniformities were a function of the combined thermal resistance of the heat pipe wall and the Fecraly/magnesium-zirconate coating. In an FBC application, the heat pipe outside wall temperature is fixed by the bed temperature and the inside wall temperature is fixed by the sodium temperature. The heat transfer into the pipe is determined by the thermal resistance of both the heat pipe wall and the protective coating on the outside diameter of the pipe. Hence, the situation that occurred during this heat pipe testing will not occur in an FBC application.

In a space radiator application, the controlling factors are the temperature of the fluid contained inside the heat pipe and the thermal resistance of the heat pipe wall. Depending on design conditions, variations in wall thermal resistance might be a potential problem. This potential problem can be avoided by appropriate design and quality control considerations.

ACKNOWLEDGEMENTS

The authors wish to acknowledge the assistance of Mr. Roger D. Carlson for many helpful dicussions during the course of the project, Mr. Angelo Mele for the photographic help provided during the project, and Ms. Verna M. Stainback for typing the report.

REFERENCES

1. K. L. Uherka, R. E. Holtz, G. A. McLennan, and E. R. Koehl, "Heat Pipe Technology for Coal-Fired Power Systems," ANL/FE-85-02 (April 1985).

2. G. A. McLennan, "ANL/HTP: A Computer Code for the Simultion of Heat Pipe Operation," ANL-83-108 (Nov. 1983).

APPENDIX A. ANL/HTP COMPUTER CALCULATIONS OF HEAT PIPE PERFORMANCE FOR EXPERIMENT CONDITIONS DESCRIBED IN SEC. 5.1†

***OPERERATING STATE REACHED, Q QMIN 6.523270E+03 7.385600E+04

AXIAL HEAT TRANSPORT = 6.5233E+03 AVERAGE PIPE TEMPERATURE = 742.08
SOURCE TEMPERATURE = 760.00 SINK TEMPERATURE = 355.68
SOURCE H = 1.000E+07 SINK H = 5.346E+02

ACTUAL SOURCE TEMPERATURE = 760.00 SINK TEMPERATURE = 355.68
ACTUAL SOURCE H COEFF = 10000000.0 SINK H COEF = 534.65
VAPOR PRESSURE = 23672. CAPILLARY PRESSURE DIFF. = 2088.
LIMITS: QV= 2.0743E+10 QS= 1.7484E+05 QE= 7.3856E+04 QB= 1.2181E+07

FLUID PRESSURES AND TEMPERATURES

	EVAP START	EVAP END	COND START	COND END
PVAP:	2.36719E+04	2.36625E+04	2.36615E+04	2.36649E+04
PLIQ:	2.15837E+04	2.15967E+04	2.16295E+04	2.16391E+04
TVAP:	742.08	742.04	742.04	742.05

TEMPERATURE DROPS

(EVAP)		(COND)		(VAPOR)	
BED TO WALL	1.440E-02	WALL TO SINK	3.621E+02	EVAP:	3.394E-02
ACROSS WALL	1.563E+01	ACROSS WALL	2.119E+01	ADIA:	3.662E-03
ACROSS WICK	2.013E+00	ACROSS WICK	2.730E+00	COND:	-1.196E-02
BOILING	2.686E-01	CONDENSING	3.638E-01		

***OPERERATING STATE REACHED, Q QMIN 6.689578E+03 7.750369E+04

AXIAL HEAT TRANSPORT = 6.6896E+03 AVERAGE PIPE TEMPERATURE = 751.75
SOURCE TEMPERATURE = 770.00 SINK TEMPERATURE = 355.68
SOURCE H = 1.000E+07 SINK H = 5.346E+02

ACTUAL SOURCE TEMPERATURE = 770.00 SINK TEMPERATURE = 355.68
ACTUAL SOURCE H COEFF = 10000000.0 SINK H COEF = 534.65
VAPOR PRESSURE = 26535. CAPILLARY PRESSURE DIFF. = 2073.
LIMITS: QV= 2.5719E+10 QS= 1.9497E+05 QE= 7.7504E+04 QB= 1.0945E+07

FLUID PRESSURES AND TEMPERATURES

	EVAP START	EVAP END	COND START	COND END
PVAP:	2.65355E+04	2.65265E+04	2.65255E+04	2.65288E+04
PLIQ:	2.44625E+04	2.44758E+04	2.45092E+04	2.45190E+04
TVAP:	751.75	751.72	751.72	751.73

TEMPERATURE DROPS

(EVAP)		(COND)		(VAPOR)	
BED TO WALL	1.465E-02	WALL TO SINK	3.713E+02	EVAP:	2.954E-02
ACROSS WALL	1.591E+01	ACROSS WALL	2.157E+01	ADIA:	3.174E-03
ACROSS WICK	2.073E+00	ACROSS WICK	2.810E+00	COND:	-1.050E-02
BOILING	2.524E-01	CONDENSING	3.420E-01		

†All tabulated quantities are in SI units, except for temperature which is given in °C.

APPENDIX A. ANL/HTP COMPUTER CALCULATIONS OF HEAT PIPE PERFORMANCE FOR EXPERIMENT CONDITIONS DESCRIBED IN SEC. 5.1 (Contd.)

***OPERERATING STATE REACHED, Q QMIN 6.855973E+03 8.124631E+04

AXIAL HEAT TRANSPORT = 6.8560E+03 AVERAGE PIPE TEMPERATURE = 761.42
SOURCE TEMPERATURE = 780.00 SINK TEMPERATURE = 355.68
SOURCE H = 1.000E+07 SINK H = 5.346E+02

ACTUAL SOURCE TEMPERATURE = 780.00 SINK TEMPERATURE = 355.68
ACTUAL SOURCE H COEFF = 10000000.0 SINK H COEF = 534.65
VAPOR PRESSURE = 29682. CAPILLARY PRESSURE DIFF. = 2058.
LIMITS: QV= 3.1757E+10 QS= 2.1696E+05 QE= 8.1246E+04 QB= 9.8519E+06

FLUID PRESSURES AND TEMPERATURES

	EVAP START	EVAP END	COND START	COND END
PVAP:	2.96818E+04	2.96735E+04	2.96726E+04	2.96756E+04
PLIQ:	2.76241E+04	2.76376E+04	2.76717E+04	2.76816E+04
TVAP:	761.42	761.40	761.40	761.41

TEMPERATURE DROPS

(EVAP)		(COND)		(VAPOR)	
BED TO WALL	1.514E-02	WALL TO SINK	3.806E+02	EVAP:	2.490E-02
ACROSS WALL	1.619E+01	ACROSS WALL	2.196E+01	ADIA:	2.686E-03
ACROSS WICK	2.132E+00	ACROSS WICK	2.891E+00	COND:	-8.789E-03
BOILING	2.375E-01	CONDENSING	3.220E-01		

***OPERERATING STATE REACHED, Q QMIN 7.022434E+03 8.508231E+04

AXIAL HEAT TRANSPORT = 7.0224E+03 AVERAGE PIPE TEMPERATURE = 771.10
SOURCE TEMPERATURE = 790.00 SINK TEMPERATURE = 355.68
SOURCE H = 1.000E+07 SINK H = 5.346E+02

ACTUAL SOURCE TEMPERATURE = 790.00 SINK TEMPERATURE = 355.68
ACTUAL SOURCE H COEFF = 10000000.0 SINK H COEF = 534.65
VAPOR PRESSURE = 33132. CAPILLARY PRESSURE DIFF. = 2042.
LIMITS: QV= 3.9054E+10 QS= 2.4094E+05 QE= 8.5082E+04 QB= 8.8840E+06

FLUID PRESSURES AND TEMPERATURES

	EVAP START	EVAP END	COND START	COND END
PVAP:	3.31321E+04	3.31241E+04	3.31234E+04	3.31262E+04
PLIQ:	3.10897E+04	3.11034E+04	3.11381E+04	3.11482E+04
TVAP:	771.10	771.08	771.08	771.08

TEMPERATURE DROPS

(EVAP)		(COND)		(VAPOR)	
BED TO WALL	1.538E-02	WALL TO SINK	3.898E+02	EVAP:	2.173E-02
ACROSS WALL	1.647E+01	ACROSS WALL	2.233E+01	ADIA:	2.197E-03
ACROSS WICK	2.193E+00	ACROSS WICK	2.973E+00	COND:	-7.568E-03
BOILING	2.239E-01	CONDENSING	3.035E-01		

APPENDIX A. ANL/HTP COMPUTER CALCULATIONS OF HEAT PIPE PERFORMANCE FOR EXPERIMENT CONDITIONS DESCRIBED IN SEC. 5.1 (Contd.)

***OPERERATING STATE REACHED, Q QMIN 7.188973E+03 8.901081E+04

AXIAL HEAT TRANSPORT = 7.1890E+03 AVERAGE PIPE TEMPERATURE = 780.78
SOURCE TEMPERATURE = 800.00 SINK TEMPERATURE = 355.68
SOURCE H = 1.000E+07 SINK H = 5.346E+02

ACTUAL SOURCE TEMPERATURE = 800.00 SINK TEMPERATURE = 355.68
ACTUAL SOURCE H COEFF = 10000000.0 SINK H COEF = 534.65
VAPOR PRESSURE = 36909. CAPILLARY PRESSURE DIFF. = 2027.
LIMITS: QV= 4.7838E+10 QS= 2.6705E+05 QE= 8.9011E+04 QB= 8.0250E+06

FLUID PRESSURES AND TEMPERATURES

	EVAP START	EVAP END	COND START	COND END
PVAP:	3.69087E+04	3.69011E+04	3.69003E+04	3.69031E+04
PLIQ:	3.48815E+04	3.48955E+04	3.49308E+04	3.49411E+04
TVAP:	780.78	780.76	780.76	780.76

TEMPERATURE DROPS

(EVAP)		(COND)		(VAPOR)	
BED TO WALL	1.587E-02	WALL TO SINK	3.990E+02	EVAP:	1.904E-02
ACROSS WALL	1.674E+01	ACROSS WALL	2.270E+01	ADIA:	1.953E-03
ACROSS WICK	2.253E+00	ACROSS WICK	3.056E+00	COND:	-6.836E-03
BOILING	2.112E-01	CONDENSING	2.864E-01		

***OPERERATING STATE REACHED, Q QMIN 7.355594E+03 9.303000E+04

AXIAL HEAT TRANSPORT = 7.3556E+03 AVERAGE PIPE TEMPERATURE = 790.46
SOURCE TEMPERATURE = 810.00 SINK TEMPERATURE = 355.68
SOURCE H = 1.000E+07 SINK H = 5.346E+02

ACTUAL SOURCE TEMPERATURE = 810.00 SINK TEMPERATURE = 355.68
ACTUAL SOURCE H COEFF = 10000000.0 SINK H COEF = 534.65
VAPOR PRESSURE = 41034. CAPILLARY PRESSURE DIFF. = 2012.
LIMITS: QV= 5.8374E+10 QS= 2.9540E+05 QE= 9.3030E+04 QB= 7.2611E+06

FLUID PRESSURES AND TEMPERATURES

	EVAP START	EVAP END	COND START	COND END
PVAP:	4.10345E+04	4.10274E+04	4.10267E+04	4.10292E+04
PLIQ:	3.90226E+04	3.90368E+04	3.90727E+04	3.90832E+04
TVAP:	790.46	790.44	790.44	790.45

TEMPERATURE DROPS

(EVAP)		(COND)		(VAPOR)	
BED TO WALL	1.611E-02	WALL TO SINK	4.083E+02	EVAP:	1.636E-02
ACROSS WALL	1.701E+01	ACROSS WALL	2.307E+01	ADIA:	1.709E-03
ACROSS WICK	2.315E+00	ACROSS WICK	3.139E+00	COND:	-5.859E-03
BOILING	1.997E-01	CONDENSING	2.705E-01		

APPENDIX A. ANL/HTP COMPUTER CALCULATIONS OF HEAT PIPE PERFORMANCE FOR EXPERIMENT CONDITIONS DESCRIBED IN SEC. 5.1 (Contd.)

***OPERERATING STATE REACHED, Q QMIN 7.522293E+03 9.713869E+04

AXIAL HEAT TRANSPORT = 7.5223E+03 AVERAGE PIPE TEMPERATURE = 800.14
SOURCE TEMPERATURE = 820.00 SINK TEMPERATURE = 355.68
SOURCE H = 1.000E+07 SINK H = 5.346E+02

ACTUAL SOURCE TEMPERATURE = 820.00 SINK TEMPERATURE = 355.68
ACTUAL SOURCE H COEFF = 10000000.0 SINK H COEF = 534.65
VAPOR PRESSURE = 45534. CAPILLARY PRESSURE DIFF. = 1997.
LIMITS: QV= 7.0965E+10 QS= 3.2616E+05 QE= 9.7139E+04 QB= 6.5306E+06

FLUID PRESSURES AND TEMPERATURES

	EVAP START	EVAP END	COND START	COND END
PVAP:	4.55342E+04	4.55274E+04	4.55268E+04	4.55293E+04
PLIQ:	4.35376E+04	4.35520E+04	4.35886E+04	4.35993E+04
TVAP:	800.14	800.13	800.12	800.13

TEMPERATURE DROPS

(EVAP)		(COND)		(VAPOR)	
BED TO WALL	1.660E-02	WALL TO SINK	4.175E+02	EVAP:	1.416E-02
ACROSS WALL	1.728E+01	ACROSS WALL	2.343E+01	ADIA:	1.465E-03
ACROSS WICK	2.377E+00	ACROSS WICK	3.224E+00	COND:	-4.883E-03
BOILING	1.887E-01	CONDENSING	2.559E-01		

***OPERERATING STATE REACHED, Q QMIN 7.689062E+03 1.013349E+05

AXIAL HEAT TRANSPORT = 7.6891E+03 AVERAGE PIPE TEMPERATURE = 809.82
SOURCE TEMPERATURE = 830.00 SINK TEMPERATURE = 355.68
SOURCE H = 1.000E+07 SINK H = 5.346E+02

ACTUAL SOURCE TEMPERATURE = 830.00 SINK TEMPERATURE = 355.68
ACTUAL SOURCE H COEFF = 10000000.0 SINK H COEF = 534.65
VAPOR PRESSURE = 50433. CAPILLARY PRESSURE DIFF. = 1981.
LIMITS: QV= 8.5958E+10 QS= 3.5946E+05 QE= 1.0133E+05 QB= 5.9732E+06

FLUID PRESSURES AND TEMPERATURES

	EVAP START	EVAP END	COND START	COND END
PVAP:	5.04328E+04	5.04262E+04	5.04256E+04	5.04280E+04
PLIQ:	4.84514E+04	4.84661E+04	4.85033E+04	4.85142E+04
TVAP:	809.82	809.81	809.81	809.81

TEMPERATURE DROPS

(EVAP)		(COND)		(VAPOR)	
BED TO WALL	1.685E-02	WALL TO SINK	4.268E+02	EVAP:	1.294E-02
ACROSS WALL	1.754E+01	ACROSS WALL	2.378E+01	ADIA:	1.221E-03
ACROSS WICK	2.440E+00	ACROSS WICK	3.309E+00	COND:	-4.395E-03
BOILING	1.787E-01	CONDENSING	2.424E-01		

APPENDIX A. ANL/HTP COMPUTER CALCULATIONS OF HEAT PIPE PERFORMANCE FOR EXPERIMENT CONDITIONS DESCRIBED IN SEC. 5.1 (Contd.)

***OPERERATING STATE REACHED, Q QMIN 7.855922E+03 1.056168E+05

AXIAL HEAT TRANSPORT = 7.8559E+03 AVERAGE PIPE TEMPERATURE = 819.51
SOURCE TEMPERATURE = 840.00 SINK TEMPERATURE = 355.68
SOURCE H = 1.000E+07 SINK H = 5.346E+02

ACTUAL SOURCE TEMPERATURE = 840.00 SINK TEMPERATURE = 355.68
ACTUAL SOURCE H COEFF = 10000000.0 SINK H COEF = 534.65
VAPOR PRESSURE = 55757. CAPILLARY PRESSURE DIFF. = 1966.
LIMITS: QV= 1.0375E+11 QS= 3.9545E+05 QE= 1.0562E+05 QB= 5.4300E+06

FLUID PRESSURES AND TEMPERATURES

	EVAP START	EVAP END	COND START	COND END
PVAP:	5.57566E+04	5.57506E+04	5.57501E+04	5.57522E+04
PLIQ:	5.37905E+04	5.38054E+04	5.38432E+04	5.38543E+04
TVAP:	819.51	819.50	819.50	819.50

TEMPERATURE DROPS

(EVAP)		(COND)		(VAPOR)	
BED TO WALL	1.733E-02	WALL TO SINK	4.361E+02	EVAP:	1.074E-02
ACROSS WALL	1.780E+01	ACROSS WALL	2.414E+01	ADIA:	9.766E-04
ACROSS WICK	2.504E+00	ACROSS WICK	3.396E+00	COND:	-3.662E-03
BOILING	1.694E-01	CONDENSING	2.297E-01		

***OPERERATING STATE REACHED, Q QMIN 8.022852E+03 1.099621E+05

AXIAL HEAT TRANSPORT = 8.0229E+03 AVERAGE PIPE TEMPERATURE = 829.20
SOURCE TEMPERATURE = 850.00 SINK TEMPERATURE = 355.68
SOURCE H = 1.000E+07 SINK H = 5.346E+02

ACTUAL SOURCE TEMPERATURE = 850.00 SINK TEMPERATURE = 355.68
ACTUAL SOURCE H COEFF = 10000000.0 SINK H COEF = 534.65
VAPOR PRESSURE = 61533. CAPILLARY PRESSURE DIFF. = 1951.
LIMITS: QV= 1.2477E+11 QS= 4.3421E+05 QE= 1.0996E+05 QB= 4.9445E+06

FLUID PRESSURES AND TEMPERATURES

	EVAP START	EVAP END	COND START	COND END
PVAP:	6.15331E+04	6.15275E+04	6.15269E+04	6.15290E+04
PLIQ:	5.95822E+04	5.95974E+04	5.96359E+04	5.96471E+04
TVAP:	829.20	829.19	829.19	829.19

TEMPERATURE DROPS

(EVAP)		(COND)		(VAPOR)	
BED TO WALL	1.758E-02	WALL TO SINK	4.453E+02	EVAP:	9.277E-03
ACROSS WALL	1.805E+01	ACROSS WALL	2.448E+01	ADIA:	9.766E-04
ACROSS WICK	2.569E+00	ACROSS WICK	3.483E+00	COND:	-3.174E-03
BOILING	1.609E-01	CONDENSING	2.183E-01		

APPENDIX A. ANL/HTP COMPUTER CALCULATIONS OF HEAT PIPE PERFORMANCE FOR EXPERIMENT CONDITIONS DESCRIBED IN SEC. 5.1 (Contd.)

***OPERERATING STATE REACHED, Q QMIN 8.189844E+03 1.143256E+05

AXIAL HEAT TRANSPORT = 8.1898E+03 AVERAGE PIPE TEMPERATURE = 838.89
SOURCE TEMPERATURE = 860.00 SINK TEMPERATURE = 355.68
SOURCE H = 1.000E+07 SINK H = 5.346E+02

ACTUAL SOURCE TEMPERATURE = 860.00 SINK TEMPERATURE = 355.68
ACTUAL SOURCE H COEFF = 10000000.0 SINK H COEF = 534.65
VAPOR PRESSURE = 67791. CAPILLARY PRESSURE DIFF. = 1936.
LIMITS: QV= 1.4946E+11 QS= 4.7571E+05 QE= 1.1433E+05 QB= 4.5111E+06

FLUID PRESSURES AND TEMPERATURES

	EVAP START	EVAP END	COND START	COND END
PVAP:	6.77906E+04	6.77850E+04	6.77845E+04	6.77865E+04
PLIQ:	6.58549E+04	6.58704E+04	6.59094E+04	6.59208E+04
TVAP:	838.89	838.88	838.88	838.88

TEMPERATURE DROPS

(EVAP)		(COND)		(VAPOR)	
BED TO WALL	1.807E-02	WALL TO SINK	4.546E+02	EVAP:	8.545E-03
ACROSS WALL	1.831E+01	ACROSS WALL	2.483E+01	ADIA:	7.324E-04
ACROSS WICK	2.634E+00	ACROSS WICK	3.572E+00	COND:	-2.930E-03
BOILING	1.533E-01	CONDENSING	2.078E-01		

***OPERERATING STATE REACHED, Q QMIN 8.356914E+03 1.187619E+05

AXIAL HEAT TRANSPORT = 8.3569E+03 AVERAGE PIPE TEMPERATURE = 848.58
SOURCE TEMPERATURE = 870.00 SINK TEMPERATURE = 355.68
SOURCE H = 1.000E+07 SINK H = 5.346E+02

ACTUAL SOURCE TEMPERATURE = 870.00 SINK TEMPERATURE = 355.68
ACTUAL SOURCE H COEFF = 10000000.0 SINK H COEF = 534.65
VAPOR PRESSURE = 74558. CAPILLARY PRESSURE DIFF. = 1920.
LIMITS: QV= 1.7845E+11 QS= 5.2030E+05 QE= 1.1876E+05 QB= 4.1214E+06

FLUID PRESSURES AND TEMPERATURES

	EVAP START	EVAP END	COND START	COND END
PVAP:	7.45584E+04	7.45529E+04	7.45524E+04	7.45544E+04
PLIQ:	7.26381E+04	7.26538E+04	7.26936E+04	7.27051E+04
TVAP:	848.58	848.57	848.57	848.57

TEMPERATURE DROPS

(EVAP)		(COND)		(VAPOR)	
BED TO WALL	1.831E-02	WALL TO SINK	4.639E+02	EVAP:	7.813E-03
ACROSS WALL	1.856E+01	ACROSS WALL	2.516E+01	ADIA:	7.324E-04
ACROSS WICK	2.700E+00	ACROSS WICK	3.661E+00	COND:	-2.686E-03
BOILING	1.460E-01	CONDENSING	1.978E-01		

Distribution for ANL-85-61

Internal:

M. J. Bernard
S. K. Bhattacharyya
J. G. Daley
R. E. Holtz (35)
P. R. Huebotter
E. R. Koehl (5)
J. L. Krazinski
R. A. Lewis
P. A. Lottes
G. A. McLennan (5)
K. M. Myles
M. Petrick
P. D. Roach
J. J. Roberts
K. L. Uherka (5)
R. A. Valentin
R. S. Zeno
S. K. Zussman
ANL Patent Dept.
ANL Contract File
ANL Libraries
TIS Files (6)

External:

DOE-TIC, for distribution per UC-90f and UC-90h (158)
Manager, Chicago Operations Office, DOE
Components Technology Division Review Committee:
  P. Alexander, Flopetrol Johnston Schlumberger, Houston
  D. J. Anthony, General Electric Co., San Jose
  A. Bishop, U. of Pittsburgh
  B. A. Boley, Northwestern U.
  R. N. Christensen, Ohio State U.
  R. Cohen, Purdue U.
  R. E. Scholl, URS/John A. Blume & Associates, San Francisco
  J. Weisman, U. of Cincinnati
Office of Coal Utilization, DOE-HQ:
  W. Bunker (5)
  J. Fairbanks
Morgantown Energy Technology Center:
  L. Carpenter (5)
  F. Crouse (5)
  N. Rekos (5)
  J. Sholes (5)
Office of Energy Systems Research, DOE-HQ:
  J. Brogan
  M. Gunn
  J. Eberhardt
Office of Nuclear Energy, DOE-HQ:
  E. Wallquist
  E. Kahn
Office of Building Energy Research and Development, DOE-HQ:
  J. Ryan
  R. Fiskum
Office of Industrial Programs, DOE-HQ:
  J. Rossmeissl
  J. Eustis
NASA-Lewis Research Center:
  M. Bailey
  D. Beremand
  J. Slaby
  R. Tew

T. Mahefkey, Wright-Patterson AFB, OH
P. Marto, Naval Postgraduate School, Monterey, CA
D. M. Ernst, Thermacore, Inc., Lancaster, PA
G. Y. Eastman, Thermacore, Inc., Lancaster, PA
J. Bledsoe, General Electric Co., King of Prussia, PA
W. Syniuta, Advanced Mechanical Technology, Inc., Newton, MA
W. Toscano, Foster-Miller Assoc., Waltham, MA
E. W. Saaski, Sigma Research, Inc., Richland, WA
E. D. Waters, Sigma Research, Inc., Richland, WA